Z. Phys. C – Particles and Fields 55, 39–61 (1992)

Zeitschrift für Physik C Particles and Fields

Studies of hadronic event structure and comparisons with QCD models at the Z^0 resonance

L3 Collaboration

B. Adeva[15], O. Adriani[14], M. Aguilar-Benitez[23], S. Ahlen[9], H. Akbari[5], J. Alcaraz[23], A. Aloisio[25], G. Alverson[10], M.G. Alviggi[25], G. Ambrosi[30], Q. An[16], H. Anderhub[42], A.L. Anderson[13], V.P. Andreev[34], T. Angelov[13], L. Antonov[37], D. Antreasyan[7], P. Arce[23], A. Arefiev[24], A. Atamanchuk[34], T. Azemoon[3], T. Aziz[8,1], P.V.K.S. Baba[16], P. Bagnaia[33], J.A. Bakken[32], L. Baksay[38], R.C. Ball[3], S. Banerjee[8], J. Bao[5], R. Barillère[15], L. Barone[33], R. Battiston[30], A. Bay[17], F. Becattini[14], U. Becker[13,42], F. Behner[42], J. Behrens[42], S. Beingessner[4], Gy.L. Bencze[11], J. Berdugo[23], P. Berges[13], B. Bertucci[30], B.L. Betev[37,42], M. Biasini[30], A. Biland[42], G.M. Bilei[30], R. Bizzarri[33], J.J. Blaising[4], P. Blömeke[1], B. Blumenfeld[5], G.J. Bobbink[2], M. Bocciolini[14], R. Bock[1], A. Böhm[1], B. Borgia[33], D. Bourilkov[37], M. Bourquin[17], D. Boutigny[4], B. Bouwens[2], E. Brambilla[25], J.G. Branson[35], I.C. Brock[31], M. Brooks[21], F. Bruyant[15], C. Buisson[22], A. Bujak[39], J.D. Burger[13], W.J. Burger[17], J.P. Burq[22], J. Busenitz[38], X.D. Cai[16], M. Capell[20], M. Caria[30], F. Carminati[14], A.M. Cartacci[14], M. Cerrada[23], F. Cesaroni[33], Y.H. Chang[13], U.K. Chaturvedi[16], M. Chemarin[22], A. Chen[44], C. Chen[6], G.M. Chen[6], H.F. Chen[18], H.S. Chen[6], J. Chen[13], M. Chen[13], M.L. Chen[3], W.Y. Chen[16], G. Chiefari[25], C.Y. Chien[5], M. Chmeissani[3], S. Chung[13], C. Civinini[14], I. Clare[13], R. Clare[13], T.E. Coan[21], H.O. Cohn[28], G. Coignet[4], N. Colino[15], A. Contin[7,15], F. Crijns[27], X.T. Cui[16], X.Y. Cui[16], T.S. Dai[13], R. D'Alessandro[14], R. de Asmundis[25], A. Degré[4], K. Deiters[13], E. Dénes[11], P. Denes[32], F. DeNotaristefani[33], M. Dhina[42], D. DiBitonto[38], M. Diemoz[33], H.R. Dimitrov[37], C. Dionisi[33,15], M.T. Dova[16], E. Drago[25], T. Driever[27], D. Duchesneau[17], P. Duinker[2], I. Duran[23], H. El Mamouni[22], A. Engler[31], F.J. Eppling[13], F.C. Erné[2], P. Extermann[17], R. Fabbretti[40], M. Fabre[42], S. Falciano[33], S.J. Fan[36], O. Fackler[20], J. Fay[22], M. Felcini[15], T. Ferguson[31], D. Fernandez[23], G. Fernandez[23], F. Ferroni[33], H. Fesefeldt[1], E. Fiandrini[30], J. Field[17], F. Filthaut[27], G. Finocchiaro[33], P.H. Fisher[5], G. Forconi[17], T. Foreman[2], K. Freudenreich[42], W. Friebel[41], M. Fukushima[13], M. Gailloud[19], Yu. Galaktionov[24,13], E. Gallo[14], S.N. Ganguli[8], P. Garcia-Abia[23], S.S. Gau[44], D. Gele[22], S. Gentile[33,15], S. Goldfarb[3], Z.F. Gong[18], E. Gonzales[23], P. Göttlicher[1], D. Goujon[17], G.Gratta[29], C. Grinnell[13], M. Gruenewald[29], C. Gu[16], M. Guanziroli[16], J.K. Guo[36], A. Gurtu[8,15], H.R. Gustafson[3], L.J. Gutay[39], K. Hangarter[1], A. Hasan[16], D. Hauschildt[2], C.F. He[36], T. Hebbeker[1], M. Hebert[35], G. Herten[13], U. Herten[1], A. Hervé[15], K. Hilgers[1], H. Hofer[42], H. Hoorani[17], G. Hu[16], G.Q. Hu[36], B Ille[22], M.M. Ilyas[16], V. Innocente[25,15], H. Janssen[15], S. Jezequel[4], B.N. Jin[6], L.W. Jones[3], A. Kasser[19], R.A. Khan[16], Yu. Kamyshkov[28], P. Kapinos[34], J.S. Kapustinsky[21], Y. Karyotakis[15,4], M. Kaur[16], S. Khokhar[16], M.N. Kienzle-Focacci[17], W.W. Kinnison[21], D. Kirkby[29], S. Kirsch[41], W. Kittel[27], A. Klimentov[13,24], A.C. König[27], O. Kornadt[1], V. Koutsenko[13,24], A. Koulbardis[34], R.W. Kraemer[31], T. Kramer[13], V.R. Krastev[37], W. Krenz[1], A. Krivshich[34], J. Krizmanic[5], K.S. Kumar[12], V. Kumar[16], A. Kunin[12,24], G. Landi[14], K. Lanius[15], D. Lanske[1], S. Lanzano[25], P. Lebrun[22], P. Lecomte[42], P. Lecoq[15], P. Le Coultre[42], D.M. Lee[21], I. Leedom[10], J.M. Le Goff[15], L. Leistam[15], R. Leiste[41], M. Lenti[14], E. Leonardi[33], J. Lettry[42], X. Leytens[2], C. Li[18,16], H.T. Li[6], P.J. Li[36], X.G. Li[6], J.Y. Liao[36], W.T. Lin[44], Z.Y. Lin[18], F.L. Linde[15,2], B. Lindemann[1], D. Linnhofer[42], Y. Liu[16], W. Lohmann[41,15], E. Longo[33], Y.S. Lu[6], J.M. Lubbers[15], K. Lübelsmeyer[1], C. Luci[15], D. Luckey[7,13], L. Ludovici[33], L. Luminari[33], W.G. Ma[18], M. MacDermott[42], P.K. Malhotra[8,**], R. Malik[16], A. Malinin[4,24], C. Maña[23], D.N. Mao[3], Y.F. Mao[6], M. Maolinbay[42], P. Marchesini[42], F. Marion[4], A. Marin[9], J.P. Martin[22], L. Martinez-Laso[15], F. Marzano[33], G.G.G. Massaro[2], T. Matsuda[13], K. Mazumdar[8], P. McBride[12], T. McMahon[39], D. McNally[42], Th. Meinholz[1], M. Merk[27], L. Merola[25], M. Meschini[14], W.J. Metzger[27], Y. Mi[16], G.B. Mills[21], Y. Mir[16], G. Mirabelli[33], J. Mnich[1], M. Möller[1], B. Monteleoni[14], R. Morand[4], S. Morganti[33], N.E. Moulai[16], R. Mount[29], S. Müller[1], A. Nadtochy[34], E. Nagy[11], M. Napolitano[25], H. Newman[29], C. Neyer[42], M.A. Niaz[16], L. Niessen[1], H. Nowak[41], G. Organtini[33], D. Pandoulas[1], S. Paoletti[14], G. Passaleva[14], S. Patricelli[25], M. Pauluzzi[30], F. Pauss[42], Y.J. Pei[1], D. Perret-Gallix[4], J. Perrier[17], A. Pevsner[5], M. Pieri[15,14], P.A. Piroué[32], F. Plasil[28], V. Plyaskin[24], M. Pohl[42], V. Pojidaev[24,14], N. Produit[17], J.M. Qian[3], K.N. Qureshi[16], R. Raghavan[8], G. Rahal-Callot[42], G. Raven[2], P. Razis[26], K. Read[28], D. Ren[42], Z. Ren[16], M. Rescigno[33], S. Reucroft[10], A. Ricker[1], S. Riemann[41], O. Rind[3], H.A. Rizvi[16], B.P. Roe[3], M. Röhner[1], S. Röhner[1], L. Romero[23], J. Rose[1], S. Rosier-Lees[4], R. Rosmalen[27], Ph. Rosselet[19], A. Rubbia[13], J.A. Rubio[15,23], H. Rykaczewski[42], M. Sachwitz[41,15], J. Salicio[15,23], J.M. Salicio[23], G.S. Sanders[21], A. Santocchia[30], M.S. Sarakinos[13], G. Sartorelli[7,16], G. Sauvage[4], V. Schegelsky[34], K. Schmiemann[1], D. Schmitz[1], P. Schmitz[1], M. Schneegans[4], H. Schopper[43], D.J. Schotanus[27], S. Shotkin[13], H.J. Schreiber[41], J. Shukla[31], R. Schulte[1], S. Schulte[1], K. Schultze[1], J. Schütte[12], J. Schwenke[1], G. Schwering[1], C. Sciacca[25], I. Scott[12], R. Sehgal[16], P.G. Seiler[40], J.C. Sens[2], L. Servoli[30], I. Sheer[35], D.Z. Shen[36], S. Shevchenko[29], X.R. Shi[29], E. Shumilov[24], V. Shoutko[24], E. Soderstrom[32], A. Sopczak[35], C. Spartiotis[5], T. Spickermann[1],

P. Spillantini[14], R. Starosta[1], M. Steuer[7,13], D.P. Stickland[32], F. Sticozzi[13], H. Stone[17], K. Strauch[12], B.C. Stringfellow[39], K. Sudhakar[8,1], G. Sultanov[16], R.L. Summer[32], L.Z. Sun[18,16], H. Suter[42], R.B. Sutton[31], J.D. Swain[16], A.A. Syed[16], X.W. Tang[6], L. Taylor[10], C. Timmermans[27], Samuel C.C. Ting[13], S.M. Ting[13], M. Tonutti[1], S.C. Tonwar[8], J. Tóth[11,15], A. Tsaregorodtsev[34], G. Tsipolitis[31], C. Tully[29], K.L. Tung[6], J. Ulbricht[42], L. Urbán[11], U. Uwer[1], E. Valente[33], R.T. Van de Walle[27], I. Vetlitsky[24], G. Viertel[42], P. Vikas[16], U. Vikas[16], M. Vivargent[4], H. Vogel[31], H. Vogt[41], G. Von Dardel[15], I. Vorobiev[24], A.A. Vorobyov[34], L. Vuilleumier[19], M. Wadhwa[16], W. Wallraff[1], C.R. Wang[18], G.H. Wang[31], J.H. Wang[6], Q.F. Wang[12], X.L. Wang[18], Y.F. Wang[14], Z.M. Wang[16,18], A. Weber[1], J. Weber[42], R. Weill[19], T.J. Wenaus[20], J. Wenninger[17], M. White[13], C. Willmott[23], F. Wittgenstein[15], D. Wright[32], R.J. Wu[6], S.X. Wu[16], Y.G. Wu[6], B.Wyslouch[13], Y.Y. Xie[36], Y.D. Xu[6], Z.Z. Xu[18], Z.L. Xue[36], D.S. Yan[36], X.J. Yan[13], B.Z. Yang[18], C.G. Yang[6], G. Yang[16], K.S. Yang[6], Q.Y. Yang[6], Z.Q. Yang[36], C.H. Ye[16], J.B. Ye[18], Q. Ye[16], S.C. Yeh[44], Z.W. Yin[36], J.M. You[16], N. Yunus[16], M. Yzerman[2], C. Zaccardelli[29], P. Zemp[42], M. Zeng[16], Y. Zeng[1], D.H. Zhang[2], Z.P. Zhang[18,16], B. Zhou[9], J.F. Zhou[1], R.Y. Zhu[29], H.L. Zhuang[6], A. Zichichi[7,15,16]

[1] I. Physikalisches Institut, RWTH, W-5100 Aachen, Federal Republic of Germany*
III. Physikalisches Institut, RWTH, W-5100 Aachen, Federal Republic of Germany*
[2] National Institute for High Energy Physics, NIKHEF, NL-1009 DB Amsterdam, The Netherlands
[3] University of Michigan, Ann Arbor, MI 48109, USA
[4] Laboratoire de Physique des Particules, LAPP, F-74519 Annecy-le-Vieux, France
[5] Johns Hopkins University, Baltimore, MD-21218, USA
[6] Institute of High Energy Physics, IHEP, Beijing, People's Republic of China
[7] INFN-Sezione di Bologna, I-40126 Bologna, Italy
[8] Tata Institute of Fundamental Research, Bombay 400 005, India
[9] Boston University, Boston, MA-02215, USA
[10] Northeastern University, Boston, MA-02115, USA
[11] Central Research Institute for Physics of the Hungarian Academy of Sciences, H-1525 Budapest 114, Hungary
[12] Havard University, Cambridge, MA-02139, USA
[13] Massachusetts Institute of Technology, Cambridge, MA-02139, USA
[14] INFN Sezione di Firenze and University of Florence, I-50125 Florence, Italy
[15] European Laboratory for Particle Physics, CERN, CH-1211 Geneva 23, Switzerland
[16] World Laboratory, FBLJA Project, CH-1211 Geneva 23, Switzerland
[17] University of Geneva, CH-1211 Geneva 4, Switzerland
[18] Chinese University of Science and Technology, USTC, Hefei, Anhui 230029, People's Republic of China
[19] University of Lausanne, CH-1015 Lausanne, Switzerland
[20] Lawrence Livermore National Laboratory, Livermore, CA-94550, USA
[21] Los Alamos National Laboratory, Los Alamos, NM-87544, USA
[22] Institut de Physique Nucléaire de Lyon, IN2P3-CNRS/Université Claude Bernard, F-69622 Villeurbanne Cedex, France
[23] Centro de Investigaciones Energeticas, Medioambientales y Tecnologicas, CIEMAT, E-28040 Madrid, Spain
[24] Institute of Theoretical and Experimental Physics, ITEP, R-117259 Moscow, Russia
[25] INFN-Sezione di Napoli and University of Naples, I-80125 Naples, Italy
[26] Department of Natural Sciences, University of Cyprus, Nicosia, Cyprus
[27] University of Nymegen and NIKHEF, NL-6525 ED Nymegen, The Netherlands
[28] Oak Ridge National Laboratory, Oak Ridge, TN-37831, USA
[29] California Institute of Technology, Pasadena, CA-91125, USA
[30] INFN-Sezione di Perugia and Università Degli Studi di Perugia, I-06100 Perugia, Italy
[31] Carnegie Mellon University, Pittsburgh, PA-15213, USA
[32] Princeton University, Princeton, NJ-08544, USA
[33] INFN-Sezione di Roma and University of Rome, "La Sapienza", I-00185 Rome, Italy
[34] Nuclear Physics Institute, St. Petersburg, Russia
[35] University of California, San Diego, CA-92182, USA
[36] Shanghai Institute of Ceramics, SIC, Shanghai, People's Republic of China
[37] Bulgarian Academy of Sciences, Institute of Mechatronics, BU-1113 Sofia, Bulgaria
[38] University of Alabama, Tuscaloosa, AL-35486, USA
[39] Purdue University, West Lafayette, IN-47907, USA
[40] Paul Scherrer Institut, PSI, CH-5232 Villigen, Switzerland
[41] Institut für Hochenergiephysik, O-1615 Zeuthen, Federal Republic of Germany
[42] Eidgenössische Technische Hochschule, ETH Zürich, CH-8093 Zürich, Switzerland
[43] University of Hamburg, W-2000 Hamburg, Federal Republic of Germany
[44] High Energy Physics Group, Taiwan, ROC

Received 27 March 1992

* Supported by the German Bundesministerium für Forschung und Technologie, FRG
** Deceased

Abstract. The structure of hadronic events from Z^0 decay is studied by measuring event shape variables, factorial moments, and the energy flow distribution. The distributions, after correction for detector effects and initial and final state radiation, are compared with the predictions of different QCD Monte Carlo programs with optimized parameter values. These Monte Carlo programs use either the second order matrix element or the parton shower evolution for the perturbative QCD calculations and use the string, the cluster, or the independent fragmentation model for hadronization. Both parton shower and $O(\alpha_s^2)$ matrix element based models with string fragmentation describe the data well. The predictions of the model based on parton shower and cluster fragmentation are also in good agreement with the data. The model with independent fragmentation gives a poor description of the energy flow distribution. The predicted energy evolutions for the mean values of thrust, sphericity, aplanarity, and charge multiplicity are compared with the data measured at different center-of-mass energies. The parton shower based models with string or cluster fragmentation are found to describe the energy dependences well while the model based on the $O(\alpha_s^2)$ calculation fails to reproduce the energy dependences of these mean values.

1 Introduction

Hadronic final states produced in e^+e^- annihilation have been studied in great detail at PEP/PETRA [1], and TRISTAN [2]. Recently, it has been shown at LEP that perturbative quantum chromodynamics (QCD) successfully accounts for many aspects of the hadronic decays of the Z^0 [3]. It is believed that the primary quarks from Z^0 decays first radiate gluons, which in turn may split into quark or gluon pairs. These quarks and gluons then fragment into observable hadrons. This process, however, is not yet completely understood. Perturbative QCD itself does not describe the fragmentation process. Instead, several phenomenological models have been developed to bridge partons and final state hadrons. These models provide a way to unravel the effects of fragmentation in the experimental data, which can then be compared with the perturbative QCD calculations directly.

Several Monte Carlo programs have been developed to give a general description of the process $e^+e^- \rightarrow$hadrons, incorporating different approaches of perturbative QCD with different fragmentation models. Each program has its own parameters. Tests of QCD thus depend on these parameters, and the optimization of these parameter values is the first step for testing QCD.

Among the experimental measurements sensitive to model parameters, the event shape variables which characterize the global structure of hadronic events are the simplest. They are sensitive to the parameters of perturbative QCD as well as to those of the fragmentation models. In this paper, we report on studies of hadronic event properties, specifically the measurements of global event shape variables, factorial moments, and the energy flow distribution from a large sample of hadronic decays of the Z^0 recorded by the L3 detector at LEP. The measured distributions are corrected for detector effects and initial and final state radiation. Out of sixteen event shape variables studied, three are used to optimize the parameter values in the Monte Carlo programs. With these optimized parameter values, the Monte Carlo predictions for the event shape variables, the factorial moments, and the energy flow distribution are then compared with data. The energy dependence of the models is compared with e^+e^- data at center-of-mass energies between 10 and 91 GeV.

2 The L3 detector

The L3 detector [4] covers 99% of 4π. It consists of a central tracking chamber (TEC), a high resolution electromagnetic calorimeter composed of bismuth germanium oxide (BGO) crystals, a ring of scintillation counters, a uranium and brass hadron calorimeter with proportional wire chamber readout, and a high precision muon spectrometer. These detectors are located in a 12 m diameter magnet which provides a uniform field of 0.5 T along the beam direction. Forward BGO arrays, on either side of the detector, measure the luminosity by detecting small angle Bhabha events.

For the present analysis, we use data collected in the following ranges of polar angle:

central tracking chamber:	$40° \leqq \theta \leqq 140°$,
electromagnetic calorimeter:	$11° \leqq \theta \leqq 169°$,
hadron calorimeter:	$5° \leqq \theta \leqq 175°$,
muon spectrometer:	$36° \leqq \theta \leqq 144°$,

where θ is defined with respect to the beam axis.

3 Event selection

The events used in this study were collected at the center-of-mass energy $\sqrt{s} = 91.2$ GeV during the 1991 LEP running period. The corresponding integrated luminosity is 8.3 pb^{-1}.

The primary trigger for hadronic events requires a total energy of about 15 GeV in the calorimeters. This trigger is in logical OR with a trigger using the barrel scintilliation counters and with a charged track trigger. The combined trigger efficiency for the selected hadronic events exceeds 99.9%.

Events of the type $e^+e^- \rightarrow$hadrons are selected by two independent methods: one is based on the energy measured in the electromagnetic and hadronic calorimeters; the other employs charged tracks measured in the tracking chamber. For the calorimeter based selection, we require:

- $N_{\text{cluster}} > 12$
- $0.6 < E^C/\sqrt{s} < 1.4$
- $|E_{\parallel}^C|/E^C < 0.4$
- $E_{\perp}^C/E^C < 0.4$

where E^C is the total energy observed in the calorimeters, $E_{\parallel}^C$ is the energy imbalance along the beam direction, and $E_{\perp}^C$ is the energy imbalance in the plane perpendicular to the beam direction. The cut on the number of calorimetric clusters with energy greater than 100 MeV rejects low multiplicity events such as $\tau^+\tau^-(\gamma)$ final states. These cuts select 248 100 hadronic events.

For the charged track based selection, we require:

- $N_{\text{track}} \geqq 5$
- $E^T > 0.15\sqrt{s}$
- $|E_{\parallel}^T|/E^T < 0.75$
- $E_{\perp}^T/E^T < 0.75$
- $\phi_2 < 170°$
- $|\cos\theta_{\text{thrust}}| < 0.7$

N_{track} is the number of selected tracks. E^T, $E_{\parallel}^T$, and $E_{\perp}^T$ are, respectively, the absolute momentum sum, the longitudinal and the transverse momentum imbalances computed from charged tracks. ϕ_2 is the second largest angle in the $R-\phi$ plane between two neighboring tracks. This last requirement removes the remaining 2×3-prong $\tau^+\tau^-$ events. Each track is required to have at least 40 $R-\phi$ hits (out of 62 wires), a distance of closest approach to the interaction point of less than 5 mm in the plane perpendicular to the beam axis, and a measured transverse momentum with respect to the beam direction of greater than 100 MeV. In addition, each track is required to have at least one hit in the five outermost $R-\phi$ wires. The track polar angles are taken from matched calorimetric clusters. The cut on $|\cos\theta_{\text{thrust}}|$ selects events which are well contained in the tracking chamber. A total of 169 700 events is selected.

Monte Carlo studies show that the efficiencies for the above two selections are 98.5% and 66.9% respectively. The low efficiency for the second method is due to limited coverage of the tracking chamber. The main background sources are events from $\tau^+\tau^-$ and e^+e^- + hadrons final states. Applying the same cuts to background Monte Carlo events, the contaminations in the final $e^+e^- \rightarrow$ hadrons sample are estimated to be less than 0.2% for the first selection, and to be less than 0.1% for the second selection. Therefore, they are negligible.

We measure the event shape distributions from the calorimetric clusters and the charged tracks separately. Direct comparisons between these independent methods allow one to verify the self-consistency of the data and, in turn, provide a way to check the potential systematic bias in the detector simulation.

4 Perturbative QCD, fragmentation models, and Monte Carlo programs

The $e^+e^- \rightarrow$ hadrons process is simulated by Monte Carlo programs according to four different phases:

(1) production of $q\bar{q}(\gamma)$ (electroweak),
(2) gluon radiation (perturbative QCD),
(3) hadronization of quarks and gluons (non-perturbative QCD),
(4) decays of unstable particles.

Two approaches to the modeling of perturbative QCD exist [5]. One is the matrix element method, in which Feynman diagrams are calculated exactly, order by order. Because of the technical difficulties in the calculation, only the second order matrix element is presently available. Therefore, a maximum of four partons in the final state can be produced.

The other approach is the parton shower method. In this method, an arbitrary number of partons are branched in order to yield a description of multijet events, with no explicit upper limit on the number of partons involved. It is based on the approximation of the full matrix element expression. The parton shower picture is derived either within the framework of the leading logarithmic approximation (LLA) [6], in which only the leading terms in the perturbative expansion are kept, or within the framework of the next-to-leading logarithmic approximation (NLLA) [7], in which leading corrections to the LLA are also included. There are many ambiguities in the LLA description, especially in the renormalization scheme. Therefore, the parton shower scale parameters extracted from the LLA models through comparisons with data do not correspond exactly to the QCD scale parameter $\Lambda_{\overline{MS}}$. The NLLA includes three body parton splitting in addition to the two body parton splitting in the LLA. Therefore it improves the LLA by taking into account α_s^2 terms in the splitting function.

Because QCD is not well understood at low energy scales, the fragmentation of colored quarks and gluons into colorless hadrons cannot be calculated by perturbative QCD. One needs to rely on phenomenological models. The separation between perturbative and fragmentation phases is generally characterized by an energy scale (Q_0) with a typical value of a few GeV. Three different fragmentation models [5] have been developed: the string (SF) [8], the cluster (CF) [9], and the independent (IF) [10, 11] fragmentation models.

The string model is derived from the QCD inspired idea that a color flux tube (string) is stretched between quark and anti-quark pairs, with gluons corresponding to kinks in the string. Particles are generated in the formalism of string breaking.

In the cluster model, gluons from the perturbative phase are first split into quark and anti-quark pairs. The quark and anti-quark pairs then form colorless clusters which, depending on their masses, decay either into lower mass clusters or directly into particles.

The independent fragmentation model assumes that partons fragment in isolation from each other. In this scheme, high momentum quarks evolve separately, splitting into colorless particles and other quarks. It has been shown that the independent fragmentation model fails to describe some experimental data [12, 13].

These different perturbative QCD approaches and fragmentation models have been incorporated into many Monte Carlo programs [5]. For the current analysis, we choose JETSET 7.3 PS [14], ARIADNE 3.3 [15], NLLJET 2.0 [16], JETSET 7.3 ME [14], HERWIG 5.4 [17], and COJETS 6.22 [18]. This set of Monte Carlo programs reflects wide differences in the application of perturbative QCD approaches and fragmentation processes.

Table 1. The modified string fragmentation parameters in JETSET 7.3 Monte Carlo program. Z^0 parameters are set to those published in reference [20]

Parameters	Description	L3 setting
MSTJ(11)	choice of fragmentation functions	3
MSTJ(46)	non-azimuthal gluon decay	3
MSTJ(51)	flag for Bose-Einstein correlation	1
PARJ(54)	c quark fragmentation parameter ϵ_c	-0.07
PARJ(55)	b quark fragmentation parameter ϵ_b	-0.008
PARJ(92)	Bose-Einstein correlation parameter	2.5

(1) JETSET 7.3 PS. The JETSET parton shower Monte Carlo program simulates e^+e^- annihilation into partons and the subsequent quark and gluon branchings. It is based on the improved leading logarithmic approximation with angular ordering and with the first gluon branching modified using an $O(\alpha_s)$ matrix element distribution to reproduce the 3-jet rate. Initial state radiation is included using the lowest order calculation, following the approach presented in [19]. The JETSET program provides both the string and the independent fragmentation options. Here we study the string fragmentation only. Table 1 lists the parameters which are different from their default values in our application. The Z^0 parameters are set to those presented in [20]. For c and b quarks, the Peterson fragmentation function [21] is used with the input parameters described in [22]. The light quarks are fragmented according to the Lund symmetric function [5] along the jet axis,

$$f(z) \propto \frac{1}{z}(1-z)^a \exp\left(-\frac{bm_T^2}{z}\right)$$

where z is the fraction of $E+p_L$ taken away by the resulting hadron, m_T is the transverse mass of the system, and a and b are the fragmentation parameters. The transverse momentum spectrum, p_T, of the hadron is described by the Gaussian function

$$f(p_T) \propto \exp\left(-\frac{p_T^2}{2\cdot\sigma_q^2}\right)$$

with σ_q being a free parameter. The parameters that affect hadronic event structure most are the parton shower scale Λ_{LL}, the parton shower cutoff parameter Q_0, and the fragmentation parameters a, b, and σ_q.

(2) ARIADNE 3.3. ARIADNE is a parton shower based Monte Carlo program. The perturbative QCD cascade in ARIADNE is formed in terms of two-parton systems named color dipoles. When a gluon is emitted from a dipole, the dipole is then converted into two independent dipoles. This formulation naturally incorporates some interference phenomena of perturbative QCD. ARIADNE itself does not provide functions for fragmentation and decay processes. Instead, it is interfaced to the JETSET 7.3 fragmentation and decay routines. In addition, ARIADNE uses JETSET 7.3 routines to generate the initial $q\bar{q}$ system, using the same correction for initial state radiation. The changes to the JETSET 7.3 fragmentation parameters are shown in Table 1. Only the string fragmentation is studied here. In the ARIADNE perturbative phase, there are two main parameters that affect the parton configuration most: the parton shower scale parameter Λ_{LL} and the parton shower cutoff parameter $P_T^{\min}$. The relevant fragmentation parameters are the same as those in the JETSET 7.3 PS model.

(3) NLLJET 2.0. NLLJET is a parton shower Monte Carlo program based on the next-to-leading logarithmic approximation. The initial $q\bar{q}g$ production is included according to the $O(\alpha_s^2)$ calculations for the phase space away from the singularities. The radiative correction for e^+e^- initial state radiation is included based on a formula similar to that in [19]. NLLJET itself only generates parton systems. As in ARIADNE, the fragmentation and decay processes are carried out using JETSET string fragmentation routines with the modified parameters shown in Table 1. Like the other parton shower Monte Carlo programs, NLLJET has two parameters, Λ_{NLL} and Q_0, to control the parton shower evolution, apart from the string fragmentation parameters.

(4) JETSET 7.3 ME. Besides the parton shower option, JETSET 7.3 also provides for a full $O(\alpha_s^2)$ matrix element [23] treatment of perturbative QCD. In our application, we use 'optimized perturbation theory' [24] with the renormalization scale f being 0.003 and the minimum scaled invariant mass squared of any two partons in 3- or 4-jet events, $y_{\min}$, being 0.01. The scale f is chosen so that Q^2 is above the b quark mass while $y_{\min}$ is close to the minimum allowed value that still gives a positive 2-jet production cross section. It has been shown that a small scale f gives significantly improved agreement with the data [25–27]. In addition, we apply the parametrization given in [28] for the second order corrections to the 3-jet rate. The generated partons are subsequently fragmented using the string fragmentation model. The Peterson function [21] is used for heavy quark fragmentation*, while the Lund function [5] is used for light quark fragmentation. The relevant parameters for our study are the QCD scale parameter Λ_{ME} and the fragmentation parameters σ_q, a and b of the string model.

(5) HERWIG 5.4. HERWIG is a Monte Carlo program based on parton shower simulation within the framework of the leading logarithmic approximation. It incorporates a very detailed simulation of QCD interference phenomena [29] and treatment of parton shower development. In addition to the parton shower, hard gluon emission is included for certain phase space regions using an $O(\alpha_s)$ matrix element calculation. The fragmentation is performed by a cluster model. HERWIG does not contain a mechanism for initial state photon radiation. Compared with JETSET, HERWIG has fewer parameters. The event shape variables are most sensitive to the parton shower scale parameter Λ_{LL}, the effective gluon mass m_g, and the cluster mass $M_{\max}$, which is a threshold parameter determining whether the clusters decay into hadrons or into lower mass clusters. We keep the HERWIG parameters at their default values unless otherwise specified.

* The parameters ε_b and ε_c in the Peterson function are set to 0.010 and 0.18 respectively, so that the mean energies of b and c hadrons, predicted by the parton shower model with the parameter values given in Table 1, are reproduced by the JETSET 7.3 ME model

(6) COJETS 6.22. COJETS is a Monte Carlo program which simulates the multiple gluon radiations in the leading logarithmic approximation with incoherent branching. The parton shower algorithm is corrected for the single hard gluon emission using an $O(\alpha_s)$ calculation. This simulation is integrated with the independent jet fragmentation according to the modified version of the Field-Feynman model [11]. COJETS has four free parameters in its longitudinal fragmentation function and one free parameter to control the transverse momentum spectra in the fragmentation cascade. Since quarks and gluons fragment independently, these parameters can have different values for quark and gluon jets. As in other parton shower programs, there are also the parton shower scale parameter Λ_{LL} and the parton shower termination parameter Q_0.

5 Definition of the observables

The jet structure of hadronic events can be analyzed using the global event shape variables. There are a large number of variables available with both linear and quadratic dependences on particle momenta. In this paper, we limit our study to the following global event shape variables:

(1) *Thrust* (T), *major* (T_{major}), *and minor* (T_{minor}). Thrust [31] is defined as:

$$T=\max_{a}\frac{\sum_{a}|\mathbf{p}_a\cdot\mathbf{n}|}{\sum_{a}|\mathbf{p}_a|}$$

where $\mathbf{p}_a$ is the momentum vector of particle a. The $\sum_a$ runs over all final state particles. The direction $\mathbf{n}$, which is called the thrust axis ($\mathbf{n}_{\mathrm{thrust}}$), is chosen to maximize the above expression. Major is defined in the same way as thrust but is maximized in a plane perpendicular to the thrust axis. The resulting direction is called the major axis, $\mathbf{n}_{\mathrm{major}}$. The minor axis, $\mathbf{n}_{\mathrm{minor}}$, is defined to give an orthonormal system. The minor value is the normalized sum of momenta projected onto $\mathbf{n}_{\mathrm{minor}}$.

(2) *Oblateness* (O). Oblateness [32] is the difference of the major and minor values, i.e.,

$$O=T_{\mathrm{major}}-T_{\mathrm{minor}}.$$

(3) *Minor of the narrow side* (M_{ns}). After dividing an event into two hemispheres by a plane perpendicular to the thrust axis, the transverse momentum fraction

$$f_T=\frac{\sum_{a}|\mathbf{p}_a\times\mathbf{n}_{\mathrm{thrust}}|}{\sum_{a}|\mathbf{p}_a|}$$

is calculated for each hemisphere. The hemisphere with the smaller f_T is called the narrow side, while the minor derived from the particles in this hemisphere is defined as the minor of the narrow side [33].

(4) *3-jet resolution parameters,* y_{23}^{JADE} *and* $y_{23}^{k_\perp}$. Jets are reconstructed using invariant mass ('JADE' version [34]) and scaled transverse momentum ($k_\perp$ version [35]) jet algorithms. For each pair of particles a and b, the scaled invariant mass squared

$$y_{ab}^{\mathrm{JADE}}=2E_aE_b\cdot(1-\cos\theta_{ab})/s$$

for JADE, and the scaled transverse momentum

$$y_{ab}^{k_\perp}=2\min(E_a^2,E_b^2)\,(1-\cos\theta_{ab})/s$$

for $k_\perp$ are evaluated. E_a and E_b are the energies of the particles and θ_{ab} is the angle between them. The particle pair with the lowest $y_{ab}^{\mathrm{JADE}}(y_{ab}^{k_\perp})$ is replaced by a pseudo-particle with four momentum p_a+p_b. This procedure is repeated until all $y_{ab}^{\mathrm{JADE}}(y_{ab}^{k_\perp})$ exceed the jet resolution parameter y_{cut}. The remaining pseudo-particles are called jets. The 3-jet resolution parameter $y_{23}^{\mathrm{JADE}}(y_{23}^{k_\perp})$ is defined as the maximum jet resolution parameter (y_{cut}) for which the event still has 3-jet structure.

(5) *The* 3rd (H_3), *and the* 4th (H_4) *Fox-Wolfram moments.* The l^{th} order of the Fox-Wolfram moment [36] is given by (the P_l are the Legendre polynomials):

$$H_l=\sum_{a,b}\frac{|\mathbf{p}_a||\mathbf{p}_b|}{s}P_l(\cos\theta_{ab})$$

where p_a and p_b are the momenta of particle a and b, respectively, and θ_{ab} is the angle between the two particles. The sums run over all particles in the events. In this paper, we consider only $l=3,4$.

(6) *Sphericity* (S) *and aplanarity* (A). Sphericity and aplanarity are defined using the eigenvalues of the momentum tensor [37]:

$$s^{ij}=\frac{\sum_a p_a^i p_a^j}{\sum_a p_a^2}\quad i,j=1,2,3;$$

where p_a^i is the i^{th} component of the momentum vector $\mathbf{p}_a$. Let Q_1, Q_2, and Q_3 be the eigenvalues of s^{ij} with $Q_1\leqq Q_2\leqq Q_3$. The sphericity and aplanarity are then given by:

$$S=\tfrac{3}{2}(Q_1+Q_2);\qquad A=\tfrac{3}{2}Q_1.$$

(7) *C and D parameters.* The C and D parameters are derived from the eigenvalues of the spherocity tensor [38]:

$$\theta^{ij}=\frac{\sum_a p_a^i p_a^j/|\mathbf{p}_a|}{\sum_a|\mathbf{p}_a|}\quad i,j=1,2,3;$$

They are defined in terms of the eigenvalues of θ^{ij}, λ_1,λ_2, and λ_3, as:

$$C=3(\lambda_1\lambda_2+\lambda_2\lambda_3+\lambda_3\lambda_1);\qquad D=27\lambda_1\lambda_2\lambda_3.$$

(8) *Scaled heavy* (ρ_H) *and light* (ρ_L) *jet masses.* An event is divided into two hemispheres by a plane perpendicular

to the thrust axis. The invariant masses, M_1^2 and M_2^2, of all particles in each hemisphere are calculated separately. The scaled heavy ($M_{H,t}^2/s$) and light ($M_{L,t}^2/s$) jet masses [39] are defined as:

$$\rho_H \equiv M_{H,t}^2/s = \max(M_1^2, M_2^2)/s$$

$$\rho_L \equiv M_{L,t}^2/s = \min(M_1^2, M_2^2)/s\,.$$

(9) *Charge multiplicity* n_{ch}. We define charge multiplicity n_{ch} as the number of stable charged particles that are either produced in the fragmentation or are the decay products of other unstable particles. A particle is called stable if its mean life time is longer than $3.3 \cdot 10^{-10}$ s.

The above variables characterize the event structure in different ways. Events with a narrow two jet structure have $T_{major} \sim 0$, $y_{23} \sim 0$, $S \sim 0$, $C \sim 0$, and $\rho_H \sim 0$. Isotropic events result in $T \sim 0.5$, $S \sim 1$, and $O \sim 0$, while planar events have $T_{minor} \sim 0$, $M_{ns} \sim 0$, $A \sim 0$, and $D \sim 0$. The D parameter, aplanarity A, and light jet mass ρ_L predominantly receive contributions from events with four or more jets. More information on some of these parameters can be obtained in [40].

In the calculations of event shape variables, the word 'particle' has different meanings for different measurements. For the calorimetric measurements, the reconstructed clusters (massless) are called particles, while particles include only selected tracks (massless) for the measurements based on tracking chamber information. In the case of Monte Carlo predictions (particle level) before detector simulation, all stable charged and neutral particles, including neutrons and neutrinos, are taken into account. In the calculations from calorimetric clusters and charged tracks, the center-of-mass energy $\sqrt{s}$ is replaced by the total visible energies E^C and E^T in the event, respectively.

In addition to the above event shape variables, we also study the local particle density fluctuations ('intermittency') and the energy flow distribution. The intermittency, first reported by JACEE and NA22 [41], is measured via factorial moments [42] which can be defined in one or more dimensions. In this paper, we consider only the one dimensional case. For a given phase space variable, the interval Φ of this variable is divided into M bins, each with size $\delta\phi = \Phi/M$. For each event, we count the number of particles per bin ($n_m, m = 1, \ldots, M$) and the total number of particles $N = \sum_{m=1}^{M} n_m$. The factorial moment of rank l is then defined as:

$$F_l(\delta\phi) = \frac{M^{l-1}}{\langle N \rangle^l} \left\langle \sum_{m=1}^{M} n_m (n_m - 1) \ldots (n_m - l + 1) \right\rangle$$

where the symbol $\langle \ldots \rangle$ represents the average over all events. Only those bins with the number of particles equal to or greater than l contribute to the factorial moments of rank l. In the presence of local particle density fluctuation, the factorial moments are expected to rise with decreasing bin size $\delta\phi$, while they tend to take constant values when there is no correlation between particles. In this paper, we calculate the factorial moments from the measured tracks for the events passing the track based selection. The azimuthal angle ϕ of the track, defined in the plane perpendicular to the beam axis, is chosen to be the phase space variable for this study.

To study the energy flow distribution, we use the JADE jet finding algorithm, with $y_{cut} = 0.04$, to select 3-jet events from the sample selected by the calorimeter based criteria. The jets are reconstructed from the calorimetric clusters. For every 3-jet event, we determine the event plane using the jet axes of the two most energetic jets. The momentum vectors of the calorimetric clusters are projected onto this plane. We then divide the plane azimuthally into 36 angle bins of 10°. The angle runs from the most energetic jet toward the second most and, finally, the least energetic jet. The energy flow [12] is then defined as a histogram with the value of the i-th bin:

$$F(i) = C_{nor} \sum_{m=1}^{N} E_m(i)$$

where the summation $\sum_{m=1}^{N}$ runs over all selected 3-jet events. $E_m(i)$ is the projected energy in bin i of the event m and C_{nor} is the normalization constant. It has been suggested that the energy flow is a useful tool to study interjet phenomena [43].

6 Corrections to the observables

The procedures to derive the particle level distributions from the observed data distributions are described in this section. As examples, the distributions measured using calorimetric clusters, for thrust and the 3-jet resolution parameter y_{23}^{JADE} are compared with the JETSET 7.3 PS predictions after detector simulation in Fig. 1. Similar comparisons are shown in Fig. 2 for the charged track measurements. The Monte Carlo parameters used are those described in Sect. 4. Apart from the tail of T and M_{ns}, the data are well described by the JETSET 7.3 PS Monte Carlo using the default values of the parton shower scale parameter Λ_{LL} and the fragmentation parameters σ_q, a, and b. The response of the L3 detector is modeled with the GEANT3 [44] detector simulation program which includes the effects of energy loss, particle decay, multiple scattering and showering in the detector materials and in the beam pipe. The decays of unstable particles in the detector are also taken into account by the GEANT program. Hadronic showers in the calorimeters are simulated with the GHEISHA [45] program. The simulated events are reconstructed by the same program that is used to reconstruct the data and subjected to the same selection criteria as described above.

6.1 Corrections to the event shape variables

For the Monte Carlo events, the global event shape variables are calculated before (particle level) and after (detector level) detector simulation. The calculation before the simulation takes into account all stable particles

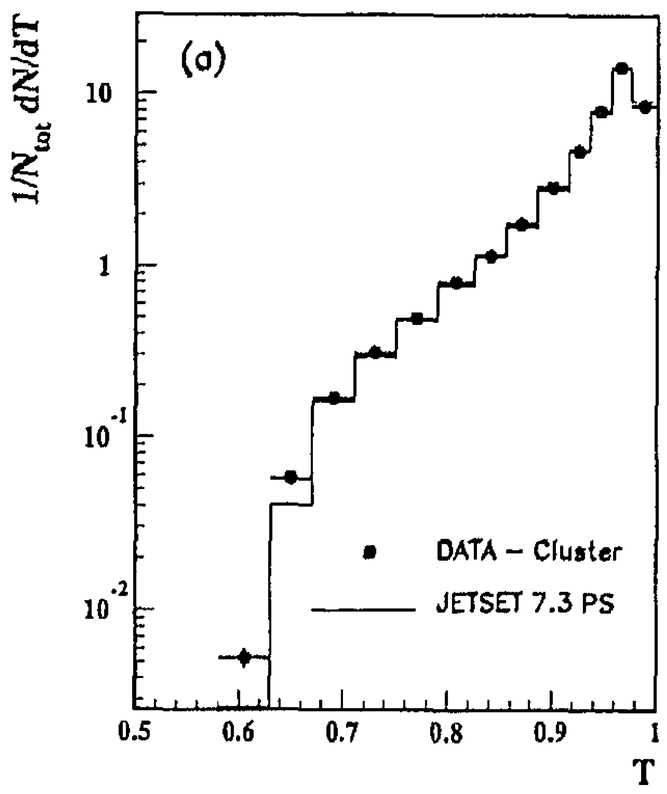

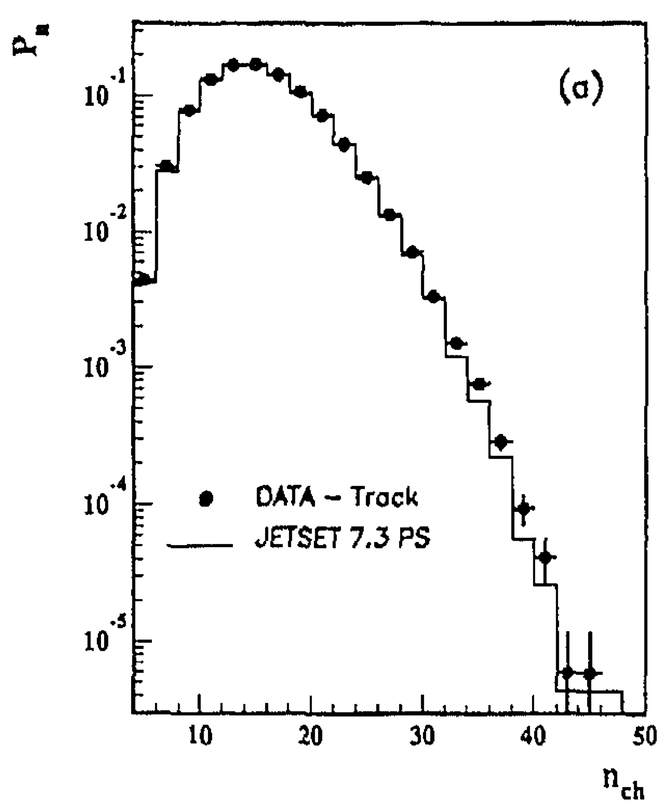

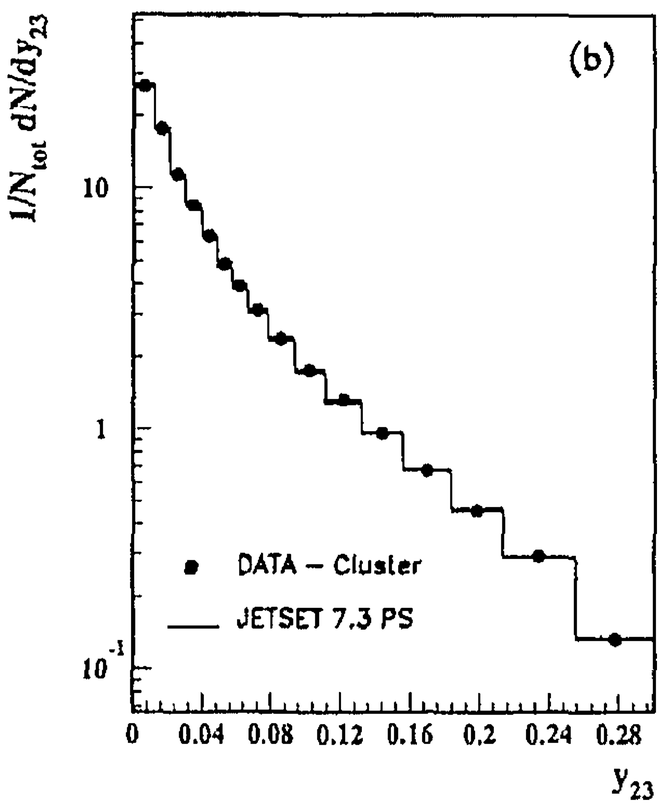

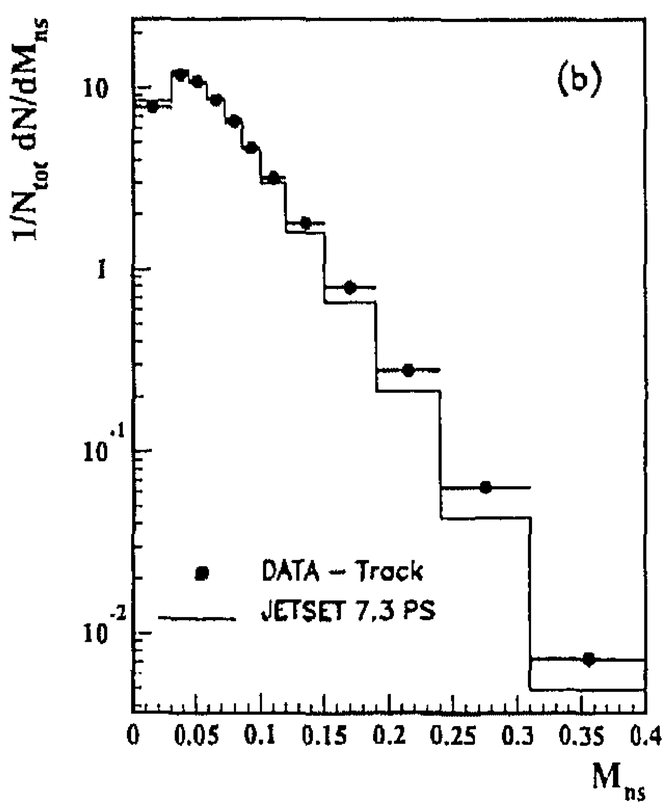

Fig. 1a, b. Comparisons between data and the JETSET 7.3 PS Monte Carlo with detector simulation using the calorimetric measurements for **a** the thrust T and **b** the 3-jet resolution parameter of the JADE algorithm y_{23}^{JADE}. Both histograms are normalized to the total number of events in the sample. The JETSET 7.3 PS parameter values differing from their defaults are shown in Table 1. Only the statistical errors are shown

Fig. 2a, b. Comparisons between data and JETSET 7.3 PS Monte Carlo with detector simulation using the charged track measurements for **a** the probability distribution for n_{ch} observed charge tracks and **b** the minor of narrow side M_{ns} distribution normalized to the total number of events in the sample. The JETSET 7.3 PS parameter values differing from their defaults are shown in Table 1. Only the statistical errors are shown

(charged and neutral) while the measured distributions employ all calorimetric clusters or charged tracks. The measured distributions at detector level differ from the true distributions at the particle level because of the detector effects, limited acceptance and finite resolution. The input distribution $f(x)$, measured distribution $g(x)$, and the detector response function $A(y,x)$ are related by the convolution integral

$$g(y)=\int A(y,x)\,f(x)\,\mathrm{d}x\,.$$

The detector effects are unfolded for global event shape variables using the regularized unfolding method as implemented in the RUN program [46]. The detector response function $A(y,x)$ is given implicitly by $\sim 300\,000$ fully simulated Monte Carlo events, each of them consisting of an input value and a measured value of the variable. These Monte Carlo events are generated using the JETSET 7.3 parton shower option together with string fragmentation and including initial and final state radiation. Apart from the parameters and flags listed in Table 1, all other parameters are set to their default values. The above convolution equation is first discretized using the spline technique [46], replacing the continuous function by a set of coefficients. It results in an equation of the form

$$g_i=\sum_j A_{ij}\,f_j$$

where g_i, A_{ij}, and f_j are discretized coefficients for $g(y)$, $A(y,x)$, and $f(x)$, respectively. The unfolding procedure is essentially a fit to find the solution f_i. In practice, unfolding by a straight-forward fit without a cut-off often

produces an unstable result due to statistical errors in the measured distribution $g(y)$. The possible spurious oscillations in the unfolding components are suppressed here by using certain *a priori* information on the degree of smoothness of the true distributions. The *a priori* information is determined by statistical methods to minimize possible biases. The acceptance corrections are naturally included in the factors. With this method, the dependences of the unfolded distributions on the Monte Carlo input distributions are small. The unfolded results are represented by a set of histograms. The bin sizes are chosen to be typically twice the detector resultions while requiring at least 100 events in the bin. For most of the bins, the differences between the unfolded and the detector level distributions are smaller than 10%.

We next generate two Monte Carlo samples with the same statistics, one with and the other without initial and final state photon emission, using the JETSET 7.3 parton shower option without detector simulation. The event shape variables are calculated for these two samples separately. We correct for radiative effect bin by bin

$$C_i^{\mathrm{rad}} = N_i^{\mathrm{off}} / N_i^{\mathrm{on}} .$$

Here N_i^{on} and N_i^{off} are the number of events in bin i for histograms with and without initial and final state photon radiation, respectively. The typical correction factors are smaller than 5%.

To estimate the systematic error on each unfolded data point, we consider the following sources: (a) the uncertainty in the detector simulation, and (b) the bias from the Monte Carlo program used for the unfolding.

Imperfections in the simulation of the calorimeters are reflected in the uncertainty of their Monte Carlo simulated energy response. To study the effects on the measured distributions, we vary the energy responses in the Monte Carlo simulation in different detector components so that the energy resolution changes by up to 10%. The variations in the measured variables are typically 2%. These differences are assigned as the systematic errors on the calorimetric measurements.

For charged track measurements, we study track reconstruction efficiency and momentum resolution along with their uncertainties, using $Z^0 \to \ell^+ \ell^- (\gamma)$ events for both data and Monte Carlo. The reference di-lepton data sample is selected from the data recorded at the same LEP running period based on the information from the electro-magnetic calorimeter, the muon chambers and the scintillation counters. The differences between the data and the Monte Carlo are then taken into account in the subsequent simulation of $e^+e^- \to$hadrons events. The uncertainties in the measured distributions due to the uncertainties in the simulation are taken as the systematic errors and are, on average, about 3%.

To account for the possible bias towards Monte Carlo input distributions in the corrections, we use a sample of 50000 fully simulated HERWIG Monte Carlo events*. The HERWIG events are reweighted so that the detector level distributions are the same as those of the data. The

* The events are generated using the HERWIG 5.3 Monte Carlo program with its default parameter values

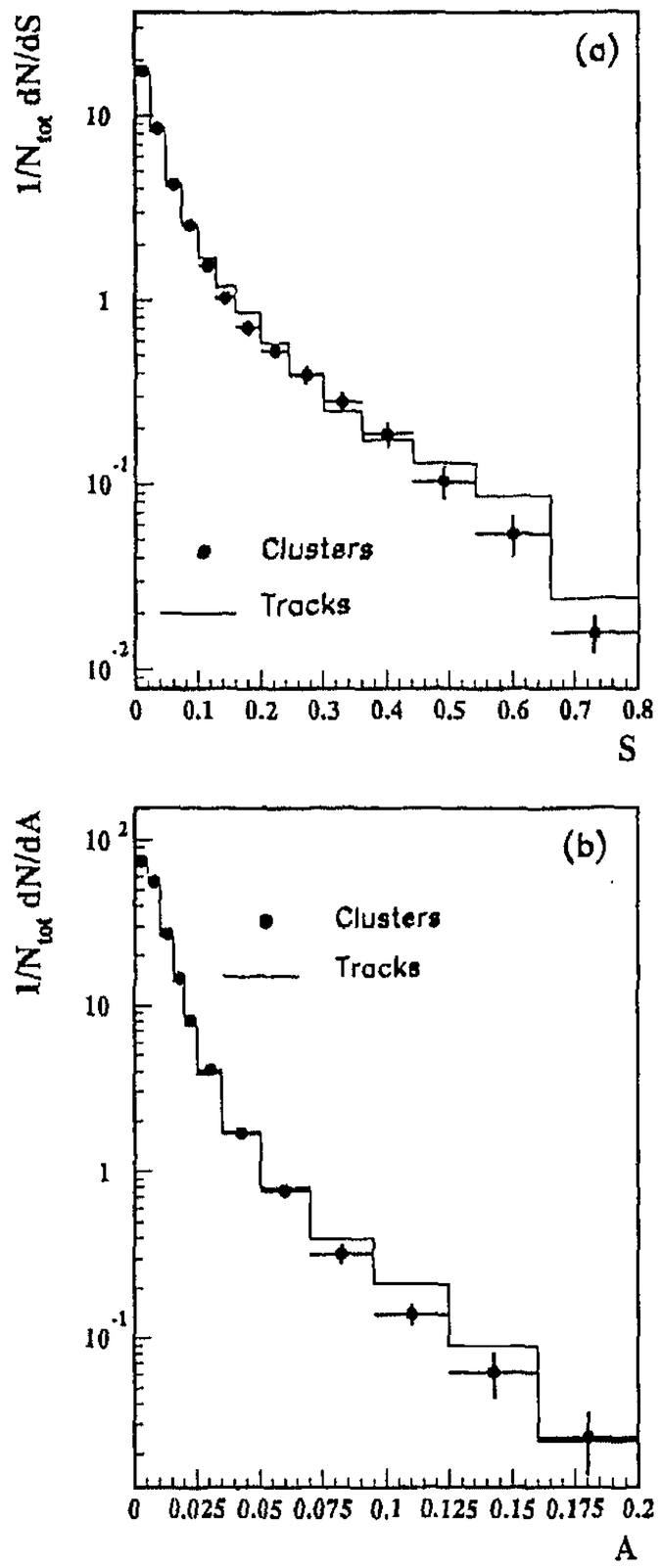

Fig. 3a, b. Comparisons between the unfolded distributions obtained from calorimeteric clusters and from charged tracks for a sphericity S and b aplanarity A. The errors on the unfolded data points from the charged tracks are not shown

reweighted HERWIG Monte Carlo events are then used as a fake data sample and unfolded by the procedure described above. We then calculate the differences between the unfolded HERWIG distributions and the reweighted HERWIG input distributions. We assign a systematic error for each unfolded data point equal to the difference for that bin. On average, the difference is 3% for both calorimetric and charged track measurements.

Finally, we compare the results from the calorimetric clusters and the charged tracks. The corrected distributions for both measurements are shown in Fig. 3 for sphericity S and aplanarity A. The two measurements agree within their errors. Similar agreement is obtained for the other variables. The good agreement demonstrates that there is no significant systematic bias from the detector simulation, in particular from calorimeter simulation. To take advantage of the small acceptance corrections for the 4π calorimeters, the unfolded distributions from the calorimetric measurements are used in the following analysis (see Tables 2–16). The charged track measurements,

Table 2. The unfolded thrust distribution. The first error is statisical, and the second one is systematic. The statistical error includes the statistical uncertainties of the data as well as of the unfolding Monte Carlo sample. The systematic error combines the uncertainties of the measurements and of the unfolding procedure

Bin	Thrust T	$1/N_{tot} \cdot dN/dT$
1	0.580 – 0.630	0.005 ± 0.001 ± 0.002
2	0.630 – 0.670	0.037 ± 0.002 ± 0.015
3	0.670 – 0.710	0.184 ± 0.009 ± 0.025
4	0.710 – 0.750	0.313 ± 0.011 ± 0.039
5	0.750 – 0.790	0.463 ± 0.017 ± 0.059
6	0.790 – 0.825	0.812 ± 0.032 ± 0.090
7	0.825 – 0.855	1.126 ± 0.032 ± 0.105
8	0.855 – 0.885	1.746 ± 0.043 ± 0.126
9	0.885 – 0.915	2.707 ± 0.067 ± 0.156
10	0.915 – 0.935	4.475 ± 0.068 ± 0.299
11	0.935 – 0.955	7.235 ± 0.117 ± 0.498
12	0.955 – 0.975	13.264 ± 0.213 ± 0.774
13	0.975 – 1.000	10.584 ± 0.092 ± 0.739
Mean Value	0.500 – 1.000	0.9364 ± 0.0003 ± 0.0021

Table 3. The unfolded major distribution

Bin	Major T_{major}	$1/N_{tot} \cdot dN/dT_{major}$
1	0.000 – 0.070	1.203 ± 0.035 ± 0.481
2	0.070 – 0.105	6.472 ± 0.048 ± 0.404
3	0.105 – 0.140	5.251 ± 0.044 ± 0.334
4	0.140 – 0.175	3.556 ± 0.034 ± 0.194
5	0.175 – 0.210	2.695 ± 0.031 ± 0.122
6	0.210 – 0.245	1.999 ± 0.022 ± 0.088
7	0.245 – 0.280	1.544 ± 0.021 ± 0.073
8	0.280 – 0.315	1.240 ± 0.018 ± 0.076
9	0.315 – 0.357	0.860 ± 0.016 ± 0.057
10	0.357 – 0.406	0.630 ± 0.010 ± 0.034
11	0.406 – 0.462	0.465 ± 0.010 ± 0.025
12	0.462 – 0.525	0.276 ± 0.006 ± 0.028
13	0.525 – 0.595	0.112 ± 0.003 ± 0.016
14	0.595 – 0.700	0.010 ± 0.001 ± 0.002
Mean Value	0.000 – 0.700	0.1749 ± 0.0005 ± 0.0050

Table 4. The unfolded minor distribution

Bin	Minor T_{minor}	$1/N_{tot} \cdot dN/dT_{minor}$
1	0.000 – 0.040	0.591 ± 0.014 ± 0.177
2	0.040 – 0.060	8.918 ± 0.124 ± 0.750
3	0.060 – 0.080	13.219 ± 0.094 ± 0.903
4	0.080 – 0.100	10.148 ± 0.081 ± 0.661
5	0.100 – 0.125	6.167 ± 0.049 ± 0.425
6	0.125 – 0.155	3.021 ± 0.030 ± 0.237
7	0.155 – 0.190	1.313 ± 0.014 ± 0.121
8	0.190 – 0.230	0.550 ± 0.008 ± 0.068
9	0.230 – 0.280	0.232 ± 0.005 ± 0.035
10	0.280 – 0.340	0.077 ± 0.002 ± 0.013
11	0.340 – 0.410	0.019 ± 0.001 ± 0.003
12	0.410 – 0.500	0.005 ± 0.001 ± 0.001
Mean Value	0.000 – 0.500	0.0938 ± 0.0002 ± 0.0022

on the other hand, are used to perform consistency checks except for the charge multiplicity distribution which is listed in Table 17. The mean charge multiplicity and the y_{23}^{JADE} distributions are in good agreement with our previously published results [47, 48]. The unfolded distributions, listed in Tables 2–17, are consistent with those reported by other LEP experiments [26, 49, 50].

Table 5. The unfolded oblateness distribution

Bin	Oblateness O	$1/N_{tot} \cdot dN/dO$
1	0.000 – 0.015	7.550 ± 0.107 ± 0.568
2	0.015 – 0.030	13.228 ± 0.067 ± 0.227
3	0.030 – 0.045	10.013 ± 0.088 ± 0.294
4	0.045 – 0.065	6.327 ± 0.093 ± 0.247
5	0.065 – 0.090	4.248 ± 0.044 ± 0.154
6	0.090 – 0.125	2.924 ± 0.052 ± 0.124
7	0.125 – 0.160	1.759 ± 0.048 ± 0.083
8	0.160 – 0.200	1.230 ± 0.027 ± 0.058
9	0.200 – 0.250	0.798 ± 0.020 ± 0.042
10	0.250 – 0.310	0.480 ± 0.015 ± 0.030
11	0.310 – 0.390	0.222 ± 0.008 ± 0.044
12	0.390 – 0.500	0.053 ± 0.002 ± 0.021
Mean Value	0.000 – 0.500	0.0806 ± 0.0004 ± 0.0018

Table 6. The unfolded distribution for minor narrow side

Bin	M_{ns}	$1/N_{tot} \cdot dN/dM_{ns}$
1	0.000 – 0.030	1.923 ± 0.169 ± 0.769
2	0.030 – 0.044	12.999 ± 0.175 ± 1.469
3	0.044 – 0.058	16.917 ± 0.449 ± 2.038
4	0.058 – 0.072	13.836 ± 0.225 ± 2.078
5	0.072 – 0.086	8.731 ± 0.218 ± 1.817
6	0.086 – 0.100	5.133 ± 0.211 ± 1.152
7	0.100 – 0.120	3.137 ± 0.075 ± 0.553
8	0.120 – 0.150	1.504 ± 0.070 ± 0.232
9	0.150 – 0.190	0.449 ± 0.033 ± 0.070
10	0.190 – 0.240	0.144 ± 0.010 ± 0.029
11	0.240 – 0.310	0.034 ± 0.003 ± 0.007
12	0.310 – 0.400	0.004 ± 0.001 ± 0.001
Mean Value	0.000 – 0.400	0.0670 ± 0.0004 ± 0.0019

Table 7. The unfolded distribution for 3-jet resolution parameter of JADE algorithm

Bin	y_{23}^{JADE}	$1/N_{tot} \cdot dN/dy_{23}^{JADE}$
1	0.000 – 0.012	26.512 ± 0.373 ± 0.745
2	0.012 – 0.021	16.885 ± 0.254 ± 0.694
3	0.021 – 0.030	11.121 ± 0.258 ± 0.664
4	0.030 – 0.039	7.633 ± 0.134 ± 0.506
5	0.039 – 0.048	5.685 ± 0.111 ± 0.358
6	0.048 – 0.057	4.737 ± 0.164 ± 0.321
7	0.057 – 0.066	3.998 ± 0.142 ± 0.257
8	0.066 – 0.078	3.430 ± 0.092 ± 0.224
9	0.078 – 0.093	2.739 ± 0.106 ± 0.201
10	0.093 – 0.111	2.030 ± 0.079 ± 0.173
11	0.111 – 0.132	1.327 ± 0.069 ± 0.132
12	0.132 – 0.156	1.065 ± 0.051 ± 0.114
13	0.156 – 0.183	0.856 ± 0.047 ± 0.097
14	0.183 – 0.213	0.553 ± 0.034 ± 0.072
15	0.213 – 0.255	0.290 ± 0.023 ± 0.042
16	0.255 – 0.300	0.160 ± 0.010 ± 0.047
Mean Value	0.000 – 0.300	0.0453 ± 0.0004 ± 0.0010

6.2 Corrections to the factorial moments and energy flow

Unlike our treatment of the event shape variables, we adopt a bin-by-bin correction method to correct for detector effects in the measured factorial moments and energy flow. Let N_i^P be the number of entries in bin-i of the input distribution at the particle level, and N_i^D be the number of entries in bin-i of the measured distribution

Table 8. The unfolded distribution for 3-jet resolution parameter of $k_\perp$ algorithm

Bin	$y_{23}^{k_\perp}$	$1/N_{tot} \cdot dN/dy_{23}^{k_\perp}$
1	0.000 – 0.012	55.881 ± 0.147 ± 0.838
2	0.012 – 0.021	10.355 ± 0.149 ± 0.337
3	0.021 – 0.030	5.795 ± 0.105 ± 0.214
4	0.030 – 0.039	3.941 ± 0.057 ± 0.134
5	0.039 – 0.048	2.706 ± 0.031 ± 0.089
6	0.048 – 0.057	2.197 ± 0.046 ± 0.103
7	0.057 – 0.066	1.787 ± 0.053 ± 0.100
8	0.066 – 0.078	1.436 ± 0.041 ± 0.089
9	0.078 – 0.093	0.966 ± 0.026 ± 0.071
10	0.093 – 0.111	0.744 ± 0.032 ± 0.066
11	0.111 – 0.132	0.577 ± 0.025 ± 0.055
12	0.132 – 0.156	0.424 ± 0.020 ± 0.045
13	0.156 – 0.183	0.313 ± 0.019 ± 0.039
14	0.183 – 0.213	0.184 ± 0.013 ± 0.041
15	0.213 – 0.255	0.103 ± 0.010 ± 0.032
16	0.255 – 0.300	0.061 ± 0.006 ± 0.024
Mean Value	0.000 – 0.300	0.0223 ± 0.0002 ± 0.0007

Table 9. The unfolded distribution for the third Fox-Wolfram moment

Bin	H_3	$1/N_{tot} \cdot dN/dH_3$
1	0.000 – 0.012	45.364 ± 0.292 ± 2.334
2	0.012 – 0.024	9.709 ± 0.061 ± 0.644
3	0.024 – 0.036	5.538 ± 0.094 ± 0.523
4	0.036 – 0.051	3.632 ± 0.095 ± 0.531
5	0.051 – 0.075	2.288 ± 0.060 ± 0.371
6	0.075 – 0.105	1.418 ± 0.023 ± 0.232
7	0.105 – 0.147	0.912 ± 0.029 ± 0.142
8	0.147 – 0.201	0.610 ± 0.015 ± 0.096
9	0.201 – 0.267	0.384 ± 0.016 ± 0.060
10	0.267 – 0.345	0.208 ± 0.009 ± 0.044
11	0.345 – 0.435	0.076 ± 0.004 ± 0.022
12	0.435 – 0.540	0.011 ± 0.001 ± 0.004
Mean Value	0.000 – 0.540	0.0417 ± 0.0004 ± 0.0022

Table 10. The unfolded distribution for the fourth Fox-Wolfram moment

Bin	H_4	$1/N_{tot} \cdot dN/dH_4$
1	0.000 – 0.100	0.203 ± 0.007 ± 0.053
2	0.100 – 0.160	0.595 ± 0.009 ± 0.034
3	0.160 – 0.220	0.656 ± 0.012 ± 0.030
4	0.220 – 0.300	0.695 ± 0.013 ± 0.041
5	0.300 – 0.380	0.764 ± 0.016 ± 0.047
6	0.380 – 0.460	0.876 ± 0.015 ± 0.047
7	0.460 – 0.540	1.105 ± 0.016 ± 0.078
8	0.540 – 0.620	1.314 ± 0.026 ± 0.091
9	0.620 – 0.700	1.720 ± 0.040 ± 0.119
10	0.700 – 0.780	2.400 ± 0.048 ± 0.216
11	0.780 – 0.880	1.779 ± 0.025 ± 0.179
12	0.880 – 1.000	0.139 ± 0.001 ± 0.014
Mean Value	0.000 – 1.000	0.5793 ± 0.0012 ± 0.0064

Table 11. The unfolded sphericity distribution

Bin	Sphericity S	$1/N_{tot} \cdot dN/dS$
1	0.000 – 0.024	17.589 ± 0.268 ± 0.536
2	0.024 – 0.048	8.552 ± 0.072 ± 0.332
3	0.048 – 0.072	4.226 ± 0.115 ± 0.220
4	0.072 – 0.100	2.542 ± 0.080 ± 0.138
5	0.100 – 0.128	1.542 ± 0.023 ± 0.088
6	0.128 – 0.160	1.025 ± 0.035 ± 0.076
7	0.160 – 0.200	0.706 ± 0.035 ± 0.056
8	0.200 – 0.244	0.525 ± 0.017 ± 0.043
9	0.244 – 0.300	0.392 ± 0.020 ± 0.038
10	0.300 – 0.360	0.279 ± 0.015 ± 0.031
11	0.360 – 0.440	0.187 ± 0.013 ± 0.025
12	0.440 – 0.540	0.103 ± 0.008 ± 0.019
13	0.540 – 0.660	0.054 ± 0.006 ± 0.012
14	0.660 – 0.800	0.016 ± 0.001 ± 0.003
Mean Value	0.000 – 0.800	0.0726 ± 0.0008 ± 0.0018

Table 12. The unfolded aplanarity distribution

Bin	Aplanarity A	$1/N_{tot} \cdot dN/dA$
1	0.000 – 0.005	74.886 ± 1.153 ± 3.034
2	0.005 – 0.010	56.015 ± 0.416 ± 2.097
3	0.010 – 0.015	27.090 ± 0.097 ± 1.422
4	0.015 – 0.020	14.596 ± 0.186 ± 1.082
5	0.020 – 0.025	8.057 ± 0.179 ± 0.616
6	0.025 – 0.035	4.048 ± 0.137 ± 0.320
7	0.035 – 0.050	1.704 ± 0.072 ± 0.121
8	0.050 – 0.070	0.769 ± 0.019 ± 0.075
9	0.070 – 0.095	0.321 ± 0.013 ± 0.041
10	0.095 – 0.125	0.139 ± 0.008 ± 0.019
11	0.125 – 0.160	0.063 ± 0.003 ± 0.019
12	0.160 – 0.200	0.025 ± 0.002 ± 0.010
Mean Value	0.000 – 0.200	0.0117 ± 0.0001 ± 0.0004

Table 13. The unfolded C parameter distribution

Bin	C Parameter	$1/N_{tot} \cdot dN/dC$
1	0.000 – 0.100	1.557 ± 0.015 ± 0.236
2	0.100 – 0.160	3.916 ± 0.013 ± 0.131
3	0.160 – 0.220	2.589 ± 0.013 ± 0.094
4	0.220 – 0.280	1.818 ± 0.008 ± 0.062
5	0.280 – 0.340	1.312 ± 0.008 ± 0.054
6	0.340 – 0.400	0.982 ± 0.007 ± 0.048
7	0.400 – 0.460	0.804 ± 0.005 ± 0.042
8	0.460 – 0.520	0.650 ± 0.005 ± 0.029
9	0.520 – 0.580	0.550 ± 0.005 ± 0.022
10	0.580 – 0.640	0.449 ± 0.003 ± 0.024
11	0.640 – 0.700	0.398 ± 0.004 ± 0.025
12	0.700 – 0.780	0.288 ± 0.003 ± 0.023
13	0.780 – 0.880	0.113 ± 0.001 ± 0.023
14	0.880 – 1.000	0.015 ± 0.001 ± 0.004
Mean Value	0.000 – 1.000	0.2599 ± 0.0004 ± 0.0053

Table 14. The unfolded D parameter distribution

Bin	D Parameter	$1/N_{tot} \cdot dN/dD$
1	0.000 – 0.016	25.739 ± 0.575 ± 1.471
2	0.016 – 0.044	8.556 ± 0.178 ± 0.465
3	0.044 – 0.088	3.166 ± 0.102 ± 0.155
4	0.088 – 0.136	1.702 ± 0.016 ± 0.094
5	0.136 – 0.188	0.931 ± 0.016 ± 0.079
6	0.188 – 0.248	0.511 ± 0.009 ± 0.041
7	0.248 – 0.320	0.278 ± 0.005 ± 0.021
8	0.320 – 0.400	0.171 ± 0.005 ± 0.014
9	0.400 – 0.500	0.082 ± 0.003 ± 0.010
10	0.500 – 0.620	0.030 ± 0.001 ± 0.005
11	0.620 – 0.800	0.017 ± 0.001 ± 0.005
Mean Value	0.000 – 0.800	0.0618 ± 0.0006 ± 0.0023

Table 15. The unfolded distribution for the scaled heavy jet mass

Bin	ρ_H	$1/N_{tot} \cdot dN/d\rho_H$
1	0.000 – 0.015	6.487 ± 0.133 ± 1.540
2	0.015 – 0.027	21.892 ± 0.073 ± 1.095
3	0.027 – 0.039	14.446 ± 0.145 ± 0.442
4	0.039 – 0.051	9.391 ± 0.090 ± 0.300
5	0.051 – 0.066	6.248 ± 0.041 ± 0.197
6	0.066 – 0.084	4.130 ± 0.051 ± 0.134
7	0.084 – 0.102	2.710 ± 0.040 ± 0.115
8	0.102 – 0.126	1.951 ± 0.028 ± 0.097
9	0.126 – 0.153	1.299 ± 0.027 ± 0.062
10	0.153 – 0.183	0.792 ± 0.021 ± 0.043
11	0.183 – 0.216	0.460 ± 0.015 ± 0.032
12	0.216 – 0.252	0.286 ± 0.010 ± 0.057
13	0.252 – 0.300	0.124 ± 0.005 ± 0.038
Mean Value	0.000 – 0.300	0.0539 ± 0.0002 ± 0.0014

Table 16. The unfolded distribution for the scaled light jet mass

Bin	ρ_L	$1/N_{tot} \cdot dN/d\rho_L$
1	0.000 – 0.006	9.943 ± 0.375 ± 3.343
2	0.006 – 0.012	43.375 ± 0.596 ± 3.142
3	0.012 – 0.018	43.335 ± 0.203 ± 2.951
4	0.018 – 0.024	26.997 ± 0.318 ± 2.234
5	0.024 – 0.030	15.514 ± 0.167 ± 1.177
6	0.030 – 0.036	8.709 ± 0.064 ± 0.592
7	0.036 – 0.045	4.896 ± 0.102 ± 0.348
8	0.045 – 0.060	2.356 ± 0.048 ± 0.214
9	0.060 – 0.078	1.192 ± 0.042 ± 0.144
10	0.078 – 0.096	0.481 ± 0.018 ± 0.064
11	0.096 – 0.120	0.135 ± 0.009 ± 0.024
Mean Value	0.000 – 0.120	0.0203 ± 0.0001 ± 0.0007

Table 17. The unfolded charge multiplicity distribution

n_{ch}	$P_n(\%)$
6	0.18 ± 0.01 ± 0.06
8	0.86 ± 0.03 ± 0.26
10	2.69 ± 0.09 ± 0.41
12	5.84 ± 0.19 ± 0.58
14	9.55 ± 0.29 ± 0.92
16	12.13 ± 0.35 ± 1.01
18	12.99 ± 0.35 ± 1.04
20	12.10 ± 0.30 ± 0.97
22	10.69 ± 0.24 ± 0.85
24	8.78 ± 0.17 ± 0.70
26	6.82 ± 0.11 ± 0.55
28	5.38 ± 0.07 ± 0.57
30	4.08 ± 0.04 ± 0.56
32	3.03 ± 0.03 ± 0.53
34	1.92 ± 0.02 ± 0.44
36	1.31 ± 0.01 ± 0.38
38	0.76 ± 0.01 ± 0.28
40	0.46 ± 0.01 ± 0.17
42	0.22 ± 0.01 ± 0.09
44	0.10 ± 0.01 ± 0.06
46	0.043 ± 0.005 ± 0.023
48	0.025 ± 0.002 ± 0.015
50	0.010 ± 0.001 ± 0.008
Mean Value	20.79 ± 0.03 ± 0.52

at detector level after detector simulation and event selection. The correction factor for bin-i is:

$$C_i^{\text{det}} = \frac{N_i^P / N^P}{N_i^D / N^D}$$

where $N^P = \sum_i N_i^P$ and $N^D = \sum_i N_i^D$. The initial and final state radiation effects are corrected in the same way as for the global event shape variables. Multiplying C_i^{det} and C_i^{rad} by the measured factorial moments or by the energy flow in bin-i (D_i), we get the corrected result in bin-i (U_i):

$$U_i = C_i^{\text{rad}} \cdot C_i^{\text{det}} \cdot D_i .$$

The correction factors C_i^{det} are obtained from the fully simulated JETSET 7.3 PS Monte Carlo events. As with the event shape variables, the errors on the corrected distributions are estimated from the uncertainties in the calorimeter and tracking chamber simulations as well as from the bias towards the input distributions of the Monte Carlo models used for calculating corrections.

7 Optimization of Monte Carlo programs

Before the direct comparisons between the data and the Monte Carlo predictions can be made, one needs to optimize parameter values of the Monte Carlo programs. We first study the dependences of the global event shape variables on the relevant parameters of the programs. Among the distributions described above, we find that the variables:

(a) the minor of the narrow side M_{ns},
(b) the 4$^{\text{th}}$ Fox-Wolfram moment H_4,
(c) the 3-jet resolution parameter of JADE algorithm y_{23}^{JADE}

together form one set of distibutions which are sensitive to all main parameters of the Monte Carlo programs. For example, in the JETSET 7.3 PS Monte Carlo, M_{ns} is sensitive to the fragmentation parameter σ_q, H_4 depends on the fragmentation parameter b, and y_{23}^{JADE} is strongly affected by $\Lambda_{\overline{\text{LL}}}$. In addition, these variables represent different algorithms in the calculations. This set of unfolded distributions is fitted to the Monte Carlo predictions to determine the 'best' values of the parameters. We note that fitting these three variables together does not eliminate the predictive capability of the programs. The comparisons between the data and the Monte Carlo distributions after optimization, for those variables not used in the optimization, provide consistency tests of the programs.

For each fit parameter, we generate Monte Carlo events, with no initial and final state photon emission and no detector simulation, for three different values around the parameter's default setting. This results in 9 Monte Carlo points for 2 fit parameters, and 27 points for 3 fit parameters. We typically generate 20000 events at $\sqrt{s} = 91.2$ GeV for each parameter point, with other parameters fixed either at their default values or at those

described in Sect. 4. Then we employ the linear interpolation method to calculate Monte Carlo predictions for other points in the multi-dimensional parameter space. We define a χ^2 as a measure of the agreement between the unfolded experimental distributions and the Monte Carlo predictions:

$$\chi^2 = \sum_i \sum_j \frac{(U_j - M_j(x))^2}{\sigma^2_{j,\mathrm{stat}} + \sigma^2_{j,\mathrm{syst}}}.$$

U_j and $M_j(x)$ are the values of the unfolded data and the Monte Carlo prediction in bin j after being normalized to the same number of events. $\sigma_{j,\mathrm{stat}}$ and $\sigma_{j,\mathrm{syst}}$ are statistical and systematic errors on the unfolded data for bin j, respectively. $\sum_i$ sums over three input distributions, while $\sum_j$ runs over all bins of the distribution. Only those bins containing more than 1% of the data events are used in the fit. The symbol x represents the set of parameters for a given Monte Carlo program. The correlations between variables and bins are not taken into account in the χ^2 calculations. The χ^2 is then minimized using the MINUIT [51] program by varying the parameters to find their 'best' values. Since all fit parameters are varied simultaneously, this procedure takes into account the correlations among the various parameters.

We use the JETSET 7.3 PS program as an example to illustrate the fit procedure in detail. The parameters that we choose to optimize are the parton shower scale parameter Λ_{LL} and the fragmentation parameters σ_q and b for various values of the parton shower termination parameter Q_0. Because of the strong correlation between parameters a and b, we vary b while keeping a at its default where. We calculate predicted JETSET 7.3 PS distributions for M_{ns}, H_4, and y_{23}^{JADE}, with Λ_{LL} varying from 0.1 GeV to 0.5 GeV, σ_q from 0.1 GeV to 0.9 GeV, and b from 0.3 GeV^{-2} to 1.0 GeV^{-2}. A total of 27 combinations in 3-dimensional parameter space are generated. For a given point (Λ_{LL}, σ_q, b) in the parameter space within the above ranges, the χ^2 is calculated for the Monte Carlo predictions interpolated from the neighboring parameter points. The 'best' parameter values are those values which give the smallest χ^2. In the case of $Q_0 = 1$ GeV, the optimized parameter values are $\Lambda_{\mathrm{LL}} = 0.30$ GeV, $\sigma_q = 0.39$ GeV, and $b = 0.76$ GeV^{-2}. The fitted parameter values and their errors are shown in Table 18 together with parameter values for $Q_0 = 2$ GeV. The uncertainties are estimated by repeating the fits removing up to five bins of the three input distributions. The optimized parameters are consistent with our previous results in [52]. They are also consistent with the default values. As can be seen in the table, the effects of early termination of the parton shower are compensated by the changes in the fragmentation paramters σ_q and b. For the optimizations of other Monte Carlo programs, we do not consider varying the parton shower termination parameter.

The ARIADNE and NLLJET programs have very similar parameters, which are also similar to those of the JETSET 7.3 PS Monte Carlo program. The parameters

Table 18. The optimized parameter values for JETSET 7.3 PS Monte Carlo program with different values of the parton shower termination parameter Q_0 (PARJ(82)). The fragmentation parameter a (PARJ(41)) is set to its default value (0.5). Other modified parameter values are listed in Table 1. Also shown is the χ^2 from the fit

Parameter	Name in the Program	$Q_0 = 1$ GeV	$Q_0 = 2$ GeV
Λ_{LL} (GeV)	PARJ(81)	0.30 ± 0.03	0.29 ± 0.03
σ_q (GeV)	PARJ(21)	0.39 ± 0.03	0.48 ± 0.05
b (GeV^{-2})	PARJ(42)	0.76 ± 0.08	0.82 ± 0.10
χ^2/(Data Points)		19.4/36	24.7/36

Table 19. The optimized parameter values for ARIADNE 3.3 Monte Carlo program with the string fragmentation. Other modified parameter values in the string fragmentation are listed in Table 1

Parameter	Name in the Program	$P_T^{\min} = 1$ GeV
Λ_{LL} (GeV)	VAR(1)	0.22 ± 0.02
σ_q (GeV)	PARJ(21)	0.50 ± 0.04
b (GeV^{-2})	PARJ(42)	0.65 ± 0.07
χ^2/(Data Points)		21.1/36

Table 20. The optimized parameter values for NLLJET 2.0 Monte Carlo program with the string fragmentation. Other modified parameter values in the string fragmentation are listed in Table 1

Parameter	Name in the Program	$Q_0 = 1$ GeV
Λ_{NLL} (GeV)	LAMBDA	0.29 ± 0.03
σ_q (GeV)	PARJ(21)	0.40 ± 0.05
b (GeV^{-2})	PARJ(42)	0.70 ± 0.10
χ^2/(Data Points)		41.3/36

Table 21. The optimized parameter values for JETSET 7.3 ME Monte Carlo program with the string fragmentation. The scale f (PARJ(129)) is chosen to be 0.003, and the recombination parameter $y_{\min}$ (PARJ(125)) in 3- or 4-jet events is set to be 0.01. Other modified parameter values in the string fragmentation are listed in Table 1

Parameter	Name in the Program	$f = 0.003$
Λ_{ME} (GeV)	PARJ(122)	0.17 ± 0.02
σ_q (GeV)	PARJ(21)	0.50 ± 0.05
b (GeV^{-2})	PARJ(42)	0.42 ± 0.06
χ^2/(Data Points)		47.6/36

Table 22. The optimized parameter values for HERWIG 5.4 Monte Carlo program with the cluster fragmentation. The effective gluon mass m_g (RMASS(13)) is set to be 0.75 GeV (default value)

Parameter	Name in the Program	$m_g = 0.75$ GeV
Λ_{LL} (GeV)	QCDLAM	0.17 ± 0.02
M_{max} (GeV)	CLMAX	3.0 ± 0.5
χ^2/(Data Point)		32.1/36

Table 23. The optimized parameter values for COJETS 6.22 Monte Carlo program with the indepenent fragmentation. Other parameters in the model are kept to their default values. Parameters d_q and d_g are kept to the same value in the optimization

Parameter	Name in the Program	Optimized Values
b_q (GeV^{-1})	FRALOQ(2)	43.0 ± 5.0
b_g (GeV^{-1})	FRALOG(2)	100.0 ± 20.0
d_q (GeV)	FRALOQ(4)	2.1 ± 0.5
d_g (GeV)	FRALOG(4)	2.1 ± 0.5
χ^2/(Data Points)		56.4/36

we optimize are the parton shower scale parameter and two string fragmentation parameters σ_q and b. The optimized values of these parameters as well as the total χ^2's from the fits are listed in Tables 19–20. The parton shower termination parameters and the fragmentation parameter a are set to their default values.

The JETSET 7.3 ME program is tuned using the renormalization scale $f=0.003$ and the recombination parameter $y_{\min}=0.01$. The parameters adjusted are the QCD scale parameter $\Lambda_{\overline{\rm ME}}$ and the string fragmentation parameters σ_q and b. The results are shown in Table 21.

For the HERWIG 5.4 program, the gluon mass m_g, which serves as the parton shower termination parameter, is fixed at 0.75 GeV. We vary the parton shower scale parameter $\Lambda_{\rm LL}$ and the maximum cluster mass $M_{\max}$ to fit the unfolded data while keeping other parameters and options to their defaults. Table 22 shows the χ^2 from the fit as well as the resulting parameter values.

The COJETS 6.22 model has a large number of free parameters involved in the fragmentation process. However, these parameters are generally correlated. To treat the program on the same footing as the others, we select only three parameters to vary in the optimization [53] while keeping other parameters at their default values. All three parameters are related to the longitudinal fragmentation. The optimized parameters, as well as their values, are shown in Table 23.

Similar optimizations have been reported by the OPAL Collaboration [49] for the JETSET 7.2 PS, HERWIG 3.4, and ARIADNE 3.1 Monte Carlo programs.

8 Comparison of the data with the models

In this section, we compare the unfolded data with the predictions of the Monte Carlo programs after optimization. This allows us to make consistent tests of the programs by comparing those distributions not used in the optimizations. For each program, we generate 100 000 events at $\sqrt{s}=91.2$ GeV with the parameter values optimized above. The JETSET 7.3 PS Monte Carlo events are generated with the parameter values adjusted for $Q_0=1$ GeV. The χ^2's between the unfolded global event shape distributions and those predicted by the Monte Carlo programs with their optimized parameters are listed in Table 24. The general structure of the events shape variables are well described by all the Monte Carlo models under study. In the following, we discuss the differences between the data and the predictions as well as the differences between predictions of the different models. In Fig. 4a–p, the unfolded event shape variables are compared with the predictions of the JETSET 7.3 PS, HERWIG 5.4, COJETS 6.22, and JETSET 7.3 ME models. These four Monte Carlo programs have wide differences in their applications of perturbative QCD and of the fragmentation process.

The predictions of JETSET 7.3 PS and ARIADNE 3.3 are generally very similar for most of the distributions. In the four or more jet dominated regions, for example at the tails of the $T_{\rm minor}$ and D parameter distributions, the predictions of these two models are systematically below the data. The predicted distributions before hadronization are already very similar. However, there is an important difference in the predicted average number of partons, with JETSET 7.3 PS predicting 9.7 while ARIADNE 3.3 predicting 5.6. In conjunction with this difference, the production rates of ARIADNE 3.3 at parton level are significantly higher than those of JETSET 7.3 PS in the narrow 2-jet regions, for example the $T\sim 1$, $y_{23}\sim 0$ regions. As indicated by the χ^2, ARIADNE 3.3 with the optimized parameter values, obtained independently of the charge multiplicity information, gives a poor description of the measured $n_{\rm ch}$ distribution. The predicted average charge multiplicity $\langle n_{\rm ch}\rangle$ is 19.1 for ARIADNE 3.3 and 21.0 for JETSET 7.3 PS, to be compared with the measured $\langle n_{\rm ch}\rangle = 20.79\pm 0.52$. For most of the event shape variables, the parton level differences in the narrow 2-jet regions are washed out by the fragmentation effects to some extent.

Variables	Nr of Bins	JETSET 7.3 PS	ARIADNE 3.3	NLLJET 2.0	HERWIG 5.4	JETSET 7.3 ME	COJETS 6.22
T	13	5.4	21.9	16.7	15.5	30.2	11.2
T_{major}	14	3.5	9.7	8.7	9.8	12.8	30.2
T_{minor}	12	22.6	24.5	54.4	21.7	23.0	26.0
O	12	15.7	13.3	21.8	3.6	37.7	107.3
M_{ns}	12	10.4	20.6	18.5	11.0	41.6	8.8
y_{23}^{JADE}	16	9.7	6.9	21.5	9.5	17.2	40.4
$y_{23}^{k_\perp}$	16	7.9	8.7	7.4	9.2	11.5	18.5
H_3	12	4.9	4.1	11.2	6.6	4.3	14.4
H_4	12	11.6	17.1	13.0	25.9	11.4	16.0
S	14	7.7	9.3	5.8	8.2	6.5	9.0
A	12	6.1	12.5	22.9	12.4	37.1	24.8
C	14	6.8	19.3	10.2	11.2	26.9	34.1
D	11	26.3	46.2	47.9	19.6	46.8	21.9
ρ_H	13	19.8	21.2	4.0	12.4	43.8	44.7
ρ_L	11	18.5	13.0	16.5	14.2	23.3	90.6
n_{ch}	20	20.5	78.2	34.9	27.8	102.5	8.8
Total	214	197.4	326.5	315.4	218.6	476.6	506.7

Table 24. χ^2 values between the unfolded data and the Monte Carlo predictions with their optimized parameter values. The statistical and systematic errors are added in quadrature in the χ^2 calculations. In the case of charge multiplicity distribution, only the data in the range $6\leqq n_{\rm ch}\leqq 44$ are compared. The data in this range amounts to 99.9% of the total sample. For $n_{\rm ch}$ outside this range, the low statistics makes the unfolding procedure less reliable. For each Monte Carlo program, 100 000 events are generated

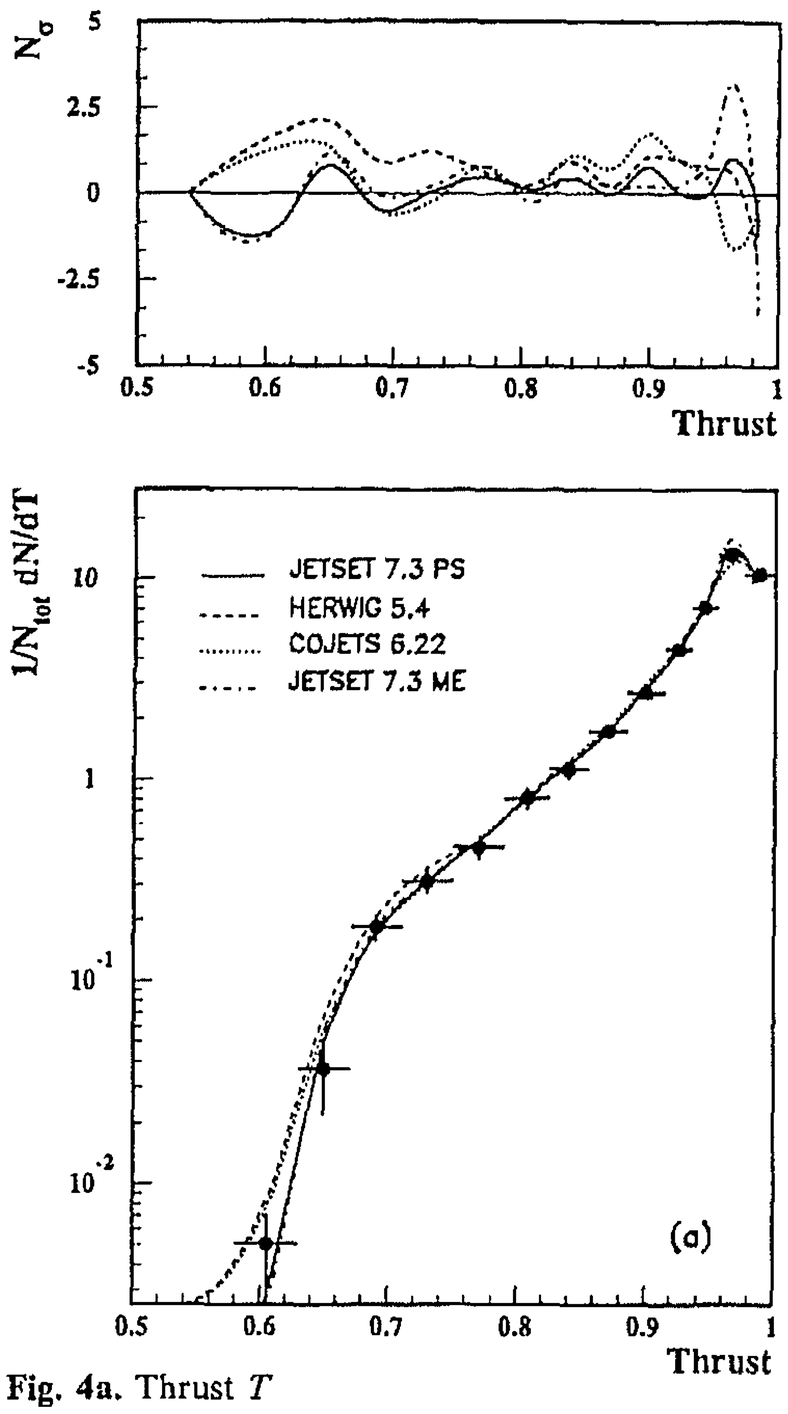

Fig. 4a. Thrust T

Fig. 4b. Major T_{major}

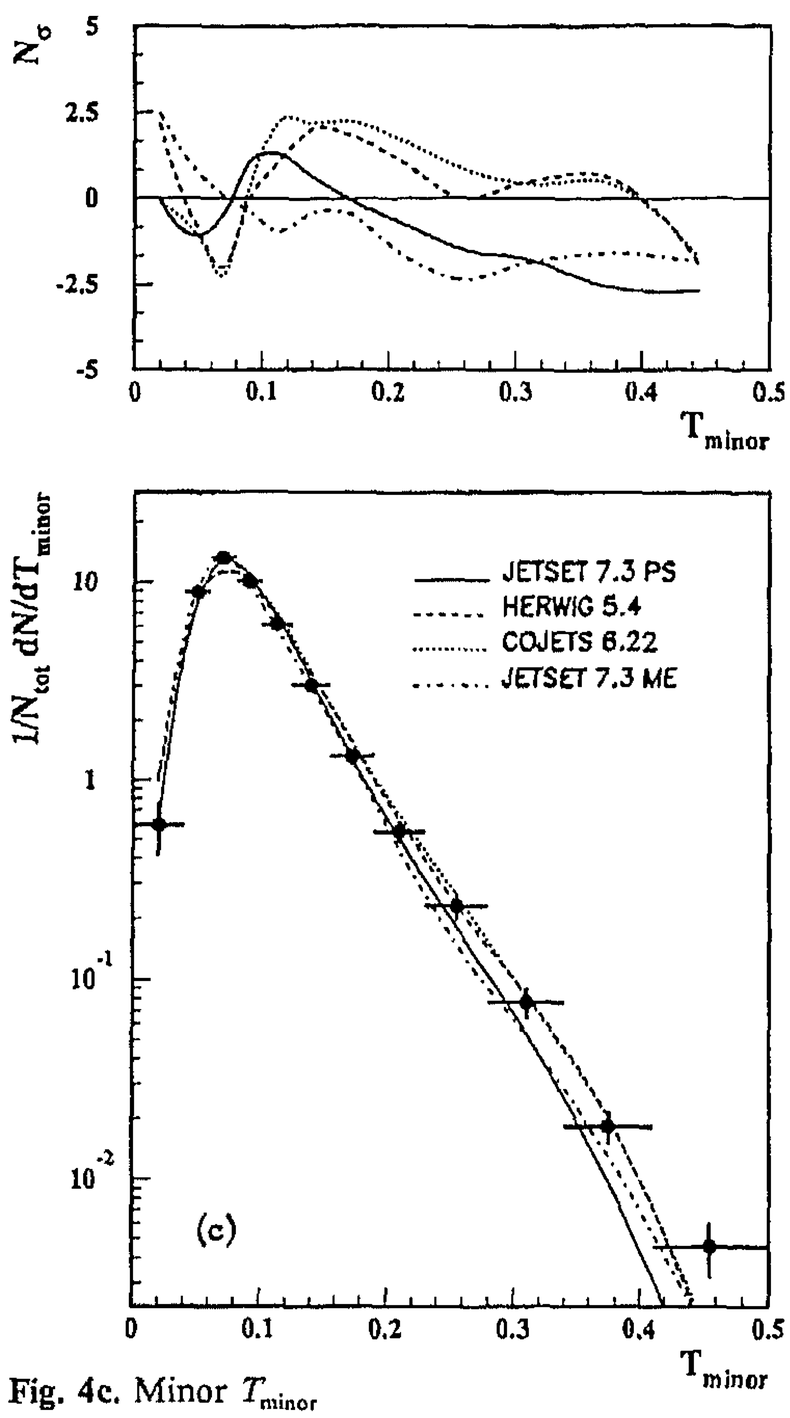

Fig. 4c. Minor T_{minor}

Fig. 4a–p. Comparisons between the unfolded data and the predictions of the JETSET 7.3 PS, HERWIG 5.4, COJETS 6.22, and JETSET 7.3 ME Monte Carlo programs with their optimized parameter values. The dots represent the data while the lines are the predictions of the Monte Carlo models. The statistical and systematic errors are added in quadrature. The top plot shows the deviations between the data and the predictions in units of errors on the unfolded data points. All histograms are normalized to the total number of events in the sample

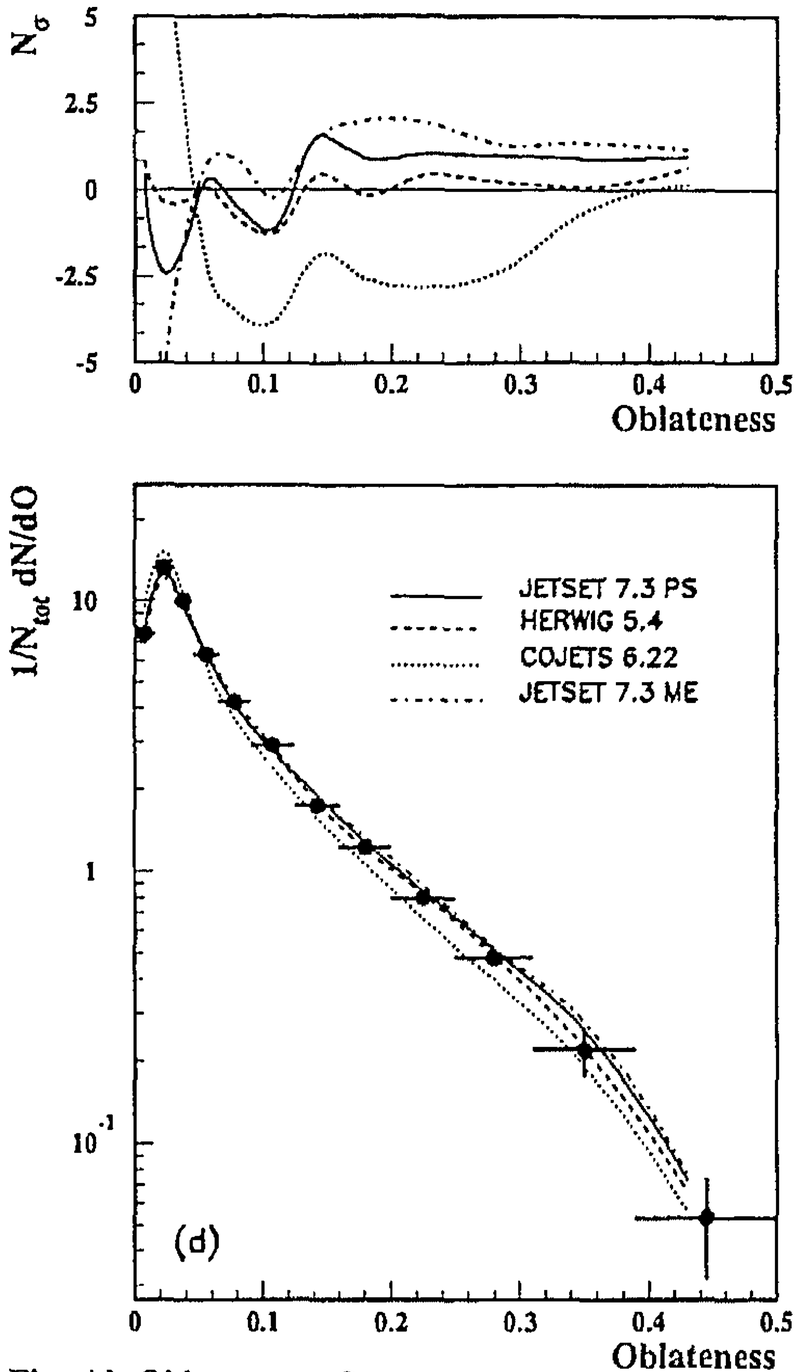

Fig. 4d. Oblatneness O

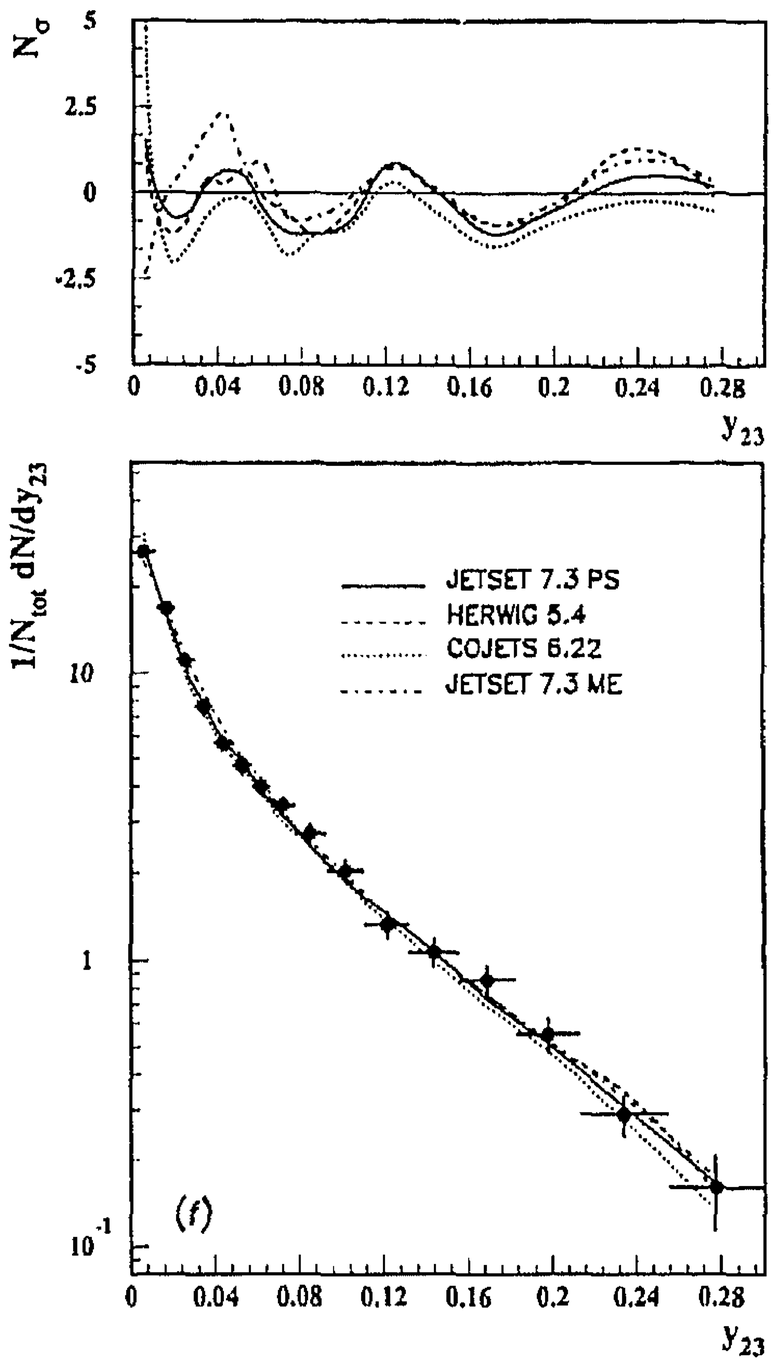

Fig. 4f. 3-jet resolution parameter of JADE algorithm y_{23}^{JADE}

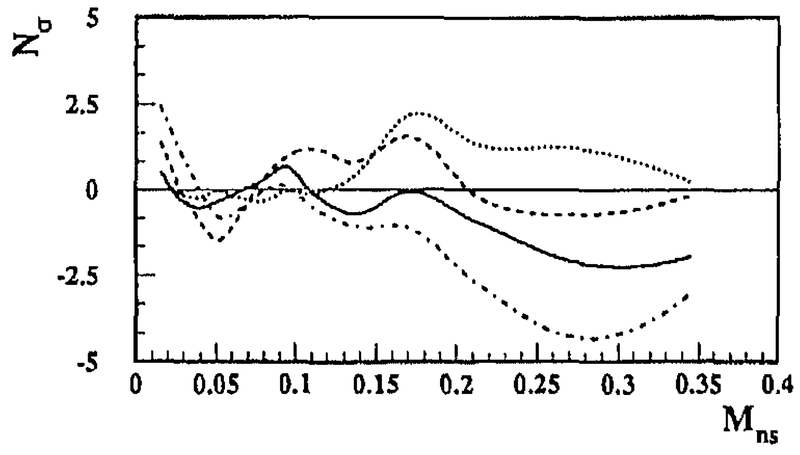

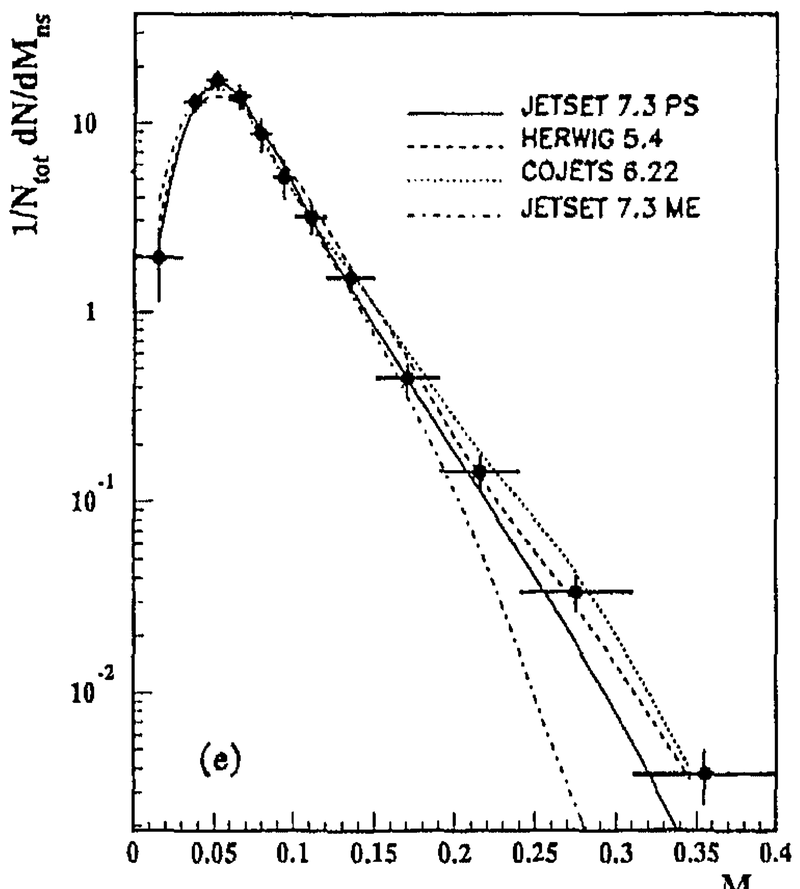

Fig. 4e. Minor of narrow side M_{ns}

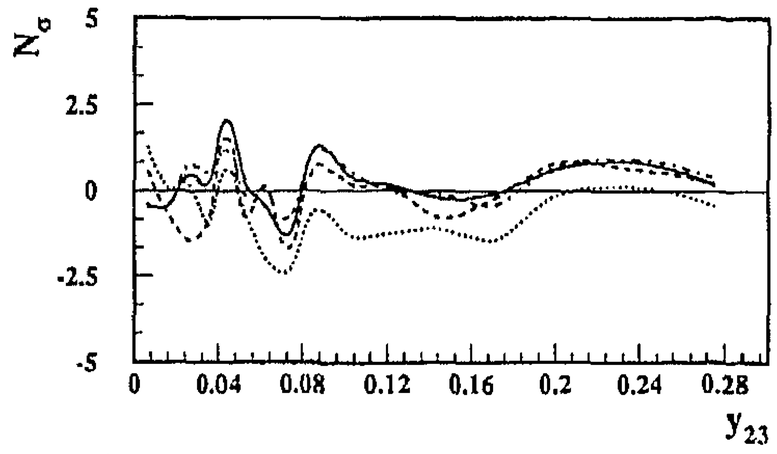

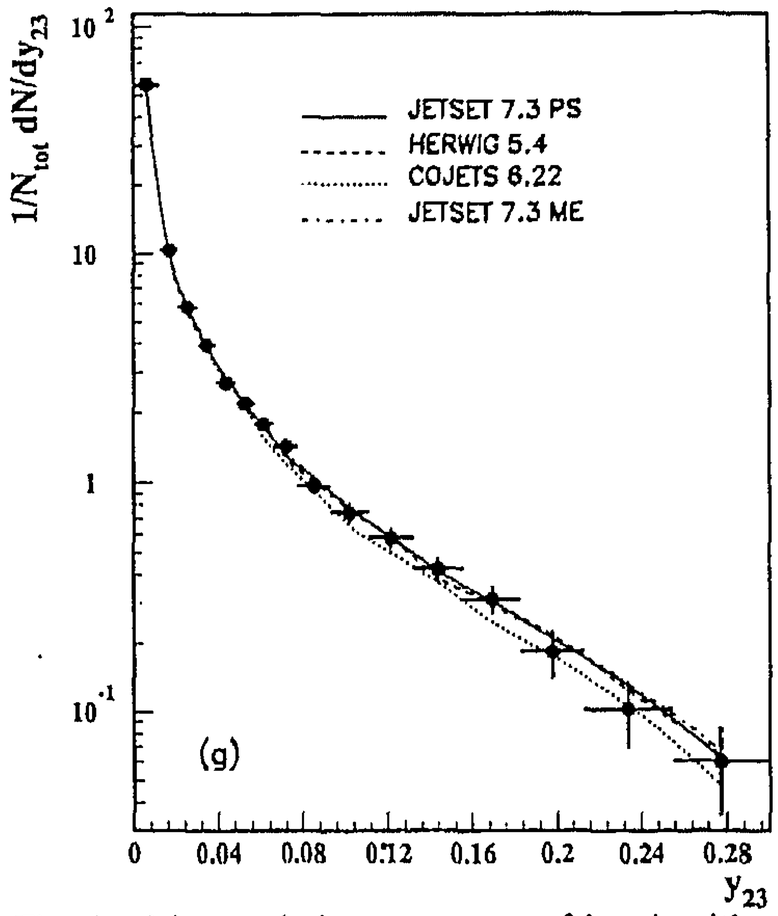

Fig. 4g. 3-jet resolution parameter of $k_\perp$ algorithm $y_{23}^{k_\perp}$

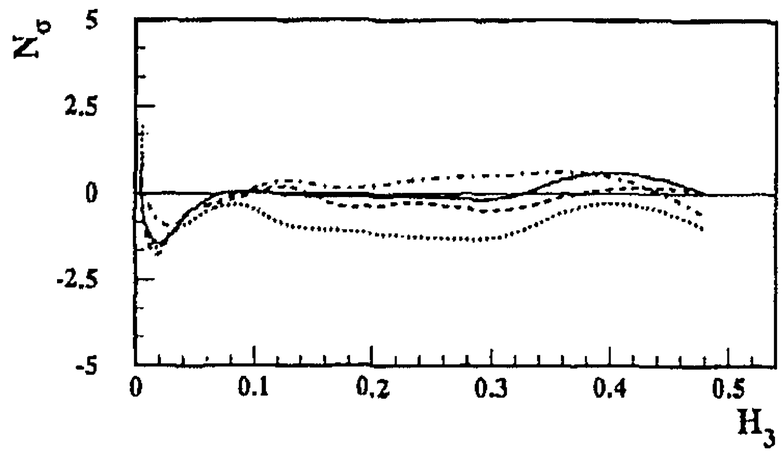

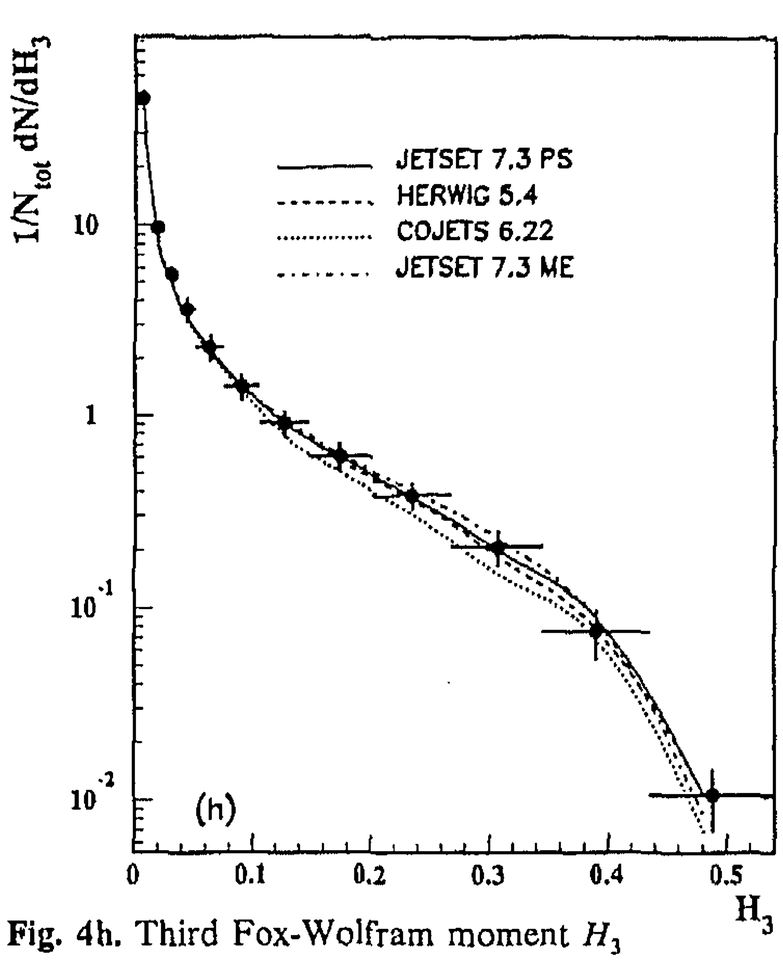

Fig. 4h. Third Fox-Wolfram moment H_3

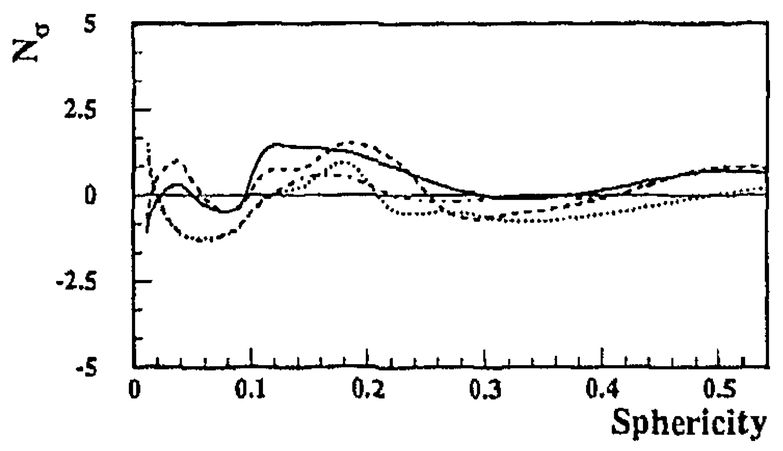

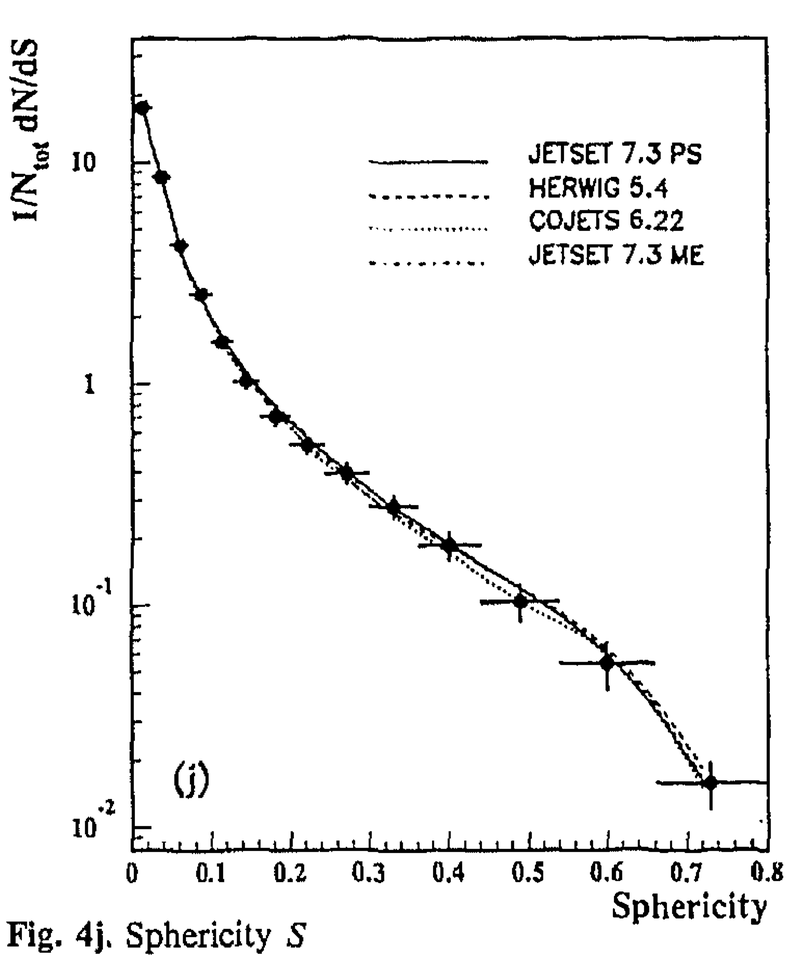

Fig. 4j. Sphericity S

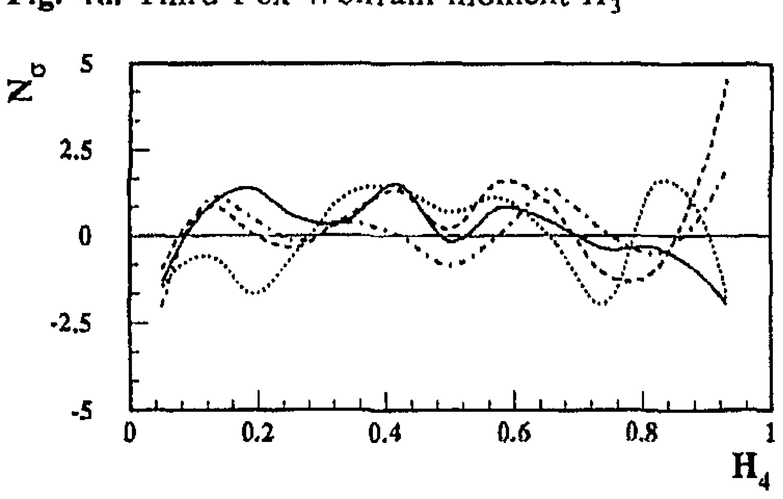

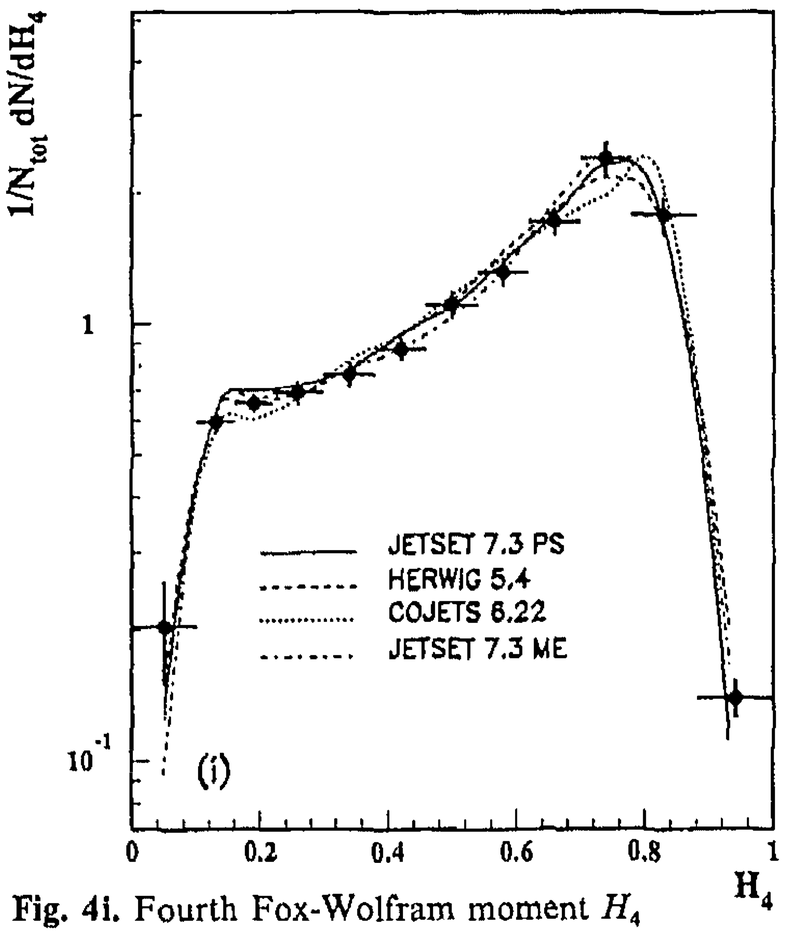

Fig. 4i. Fourth Fox-Wolfram moment H_4

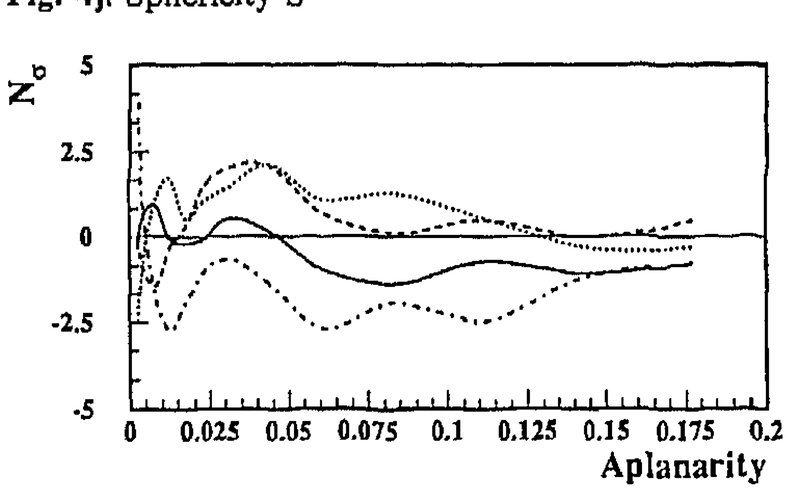

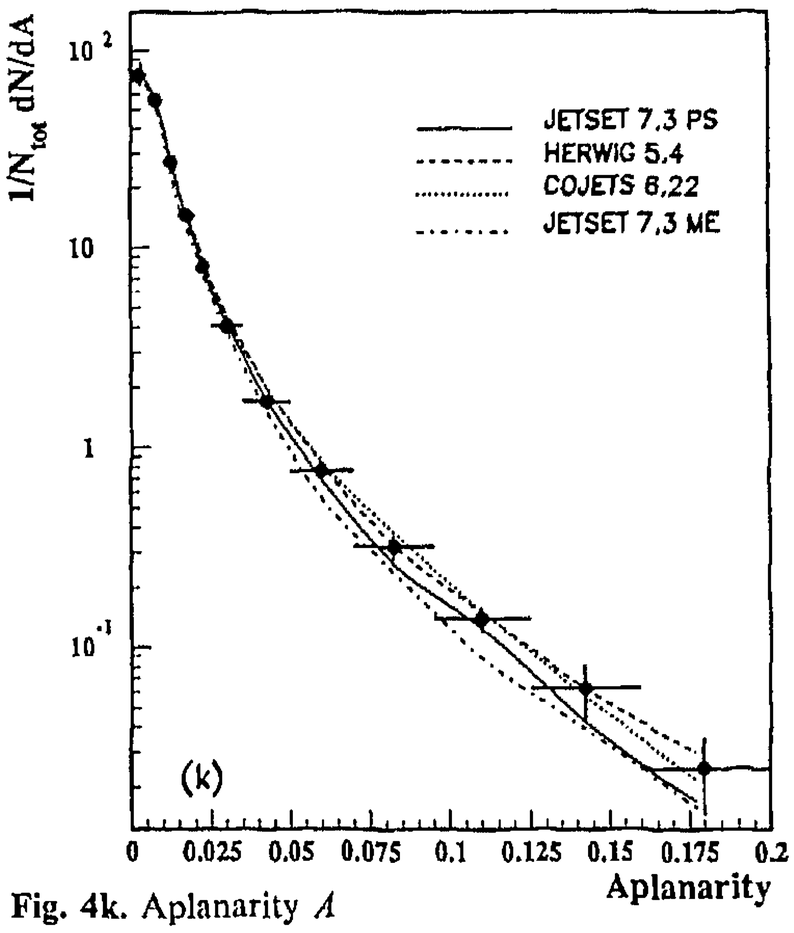

Fig. 4k. Aplanarity A

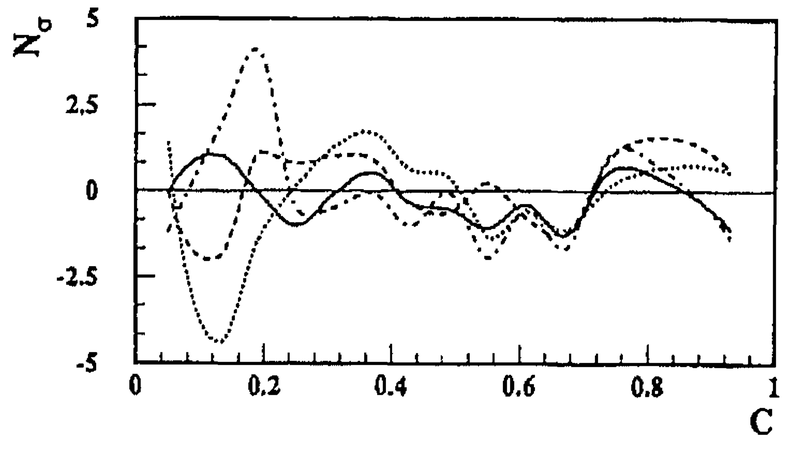

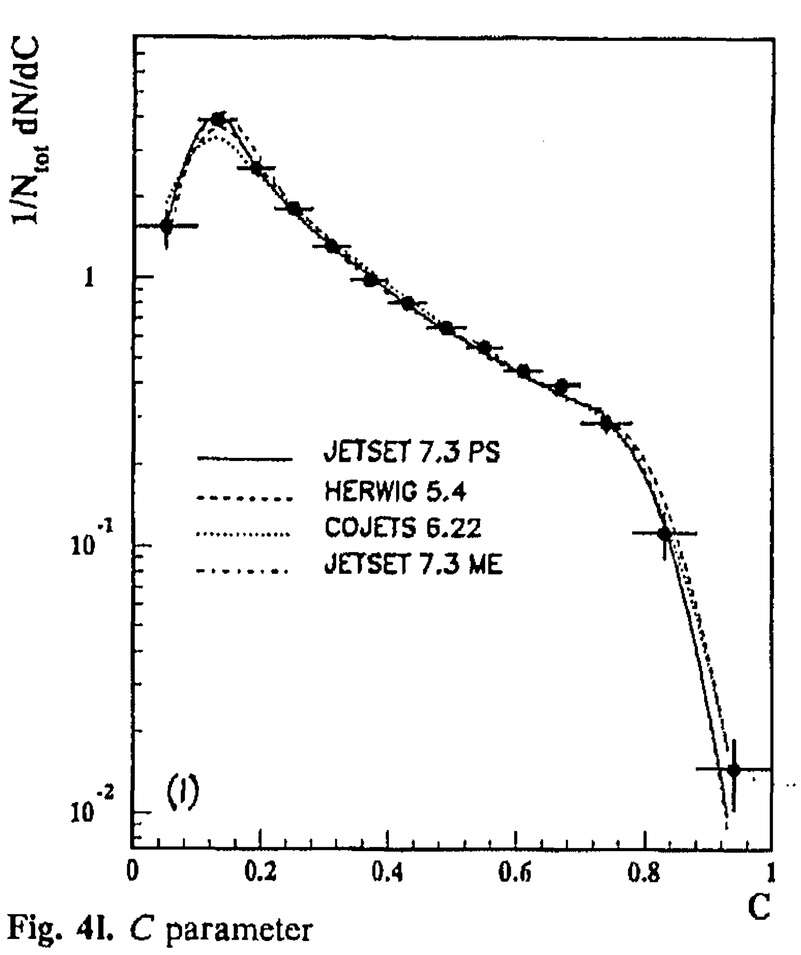

Fig. 4l. C parameter

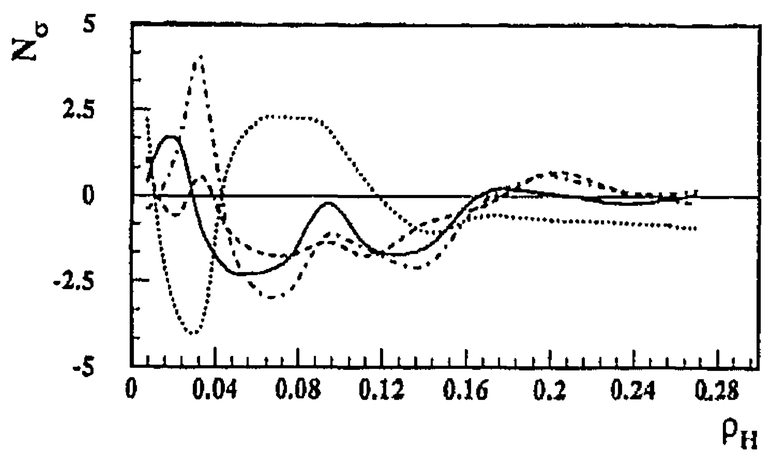

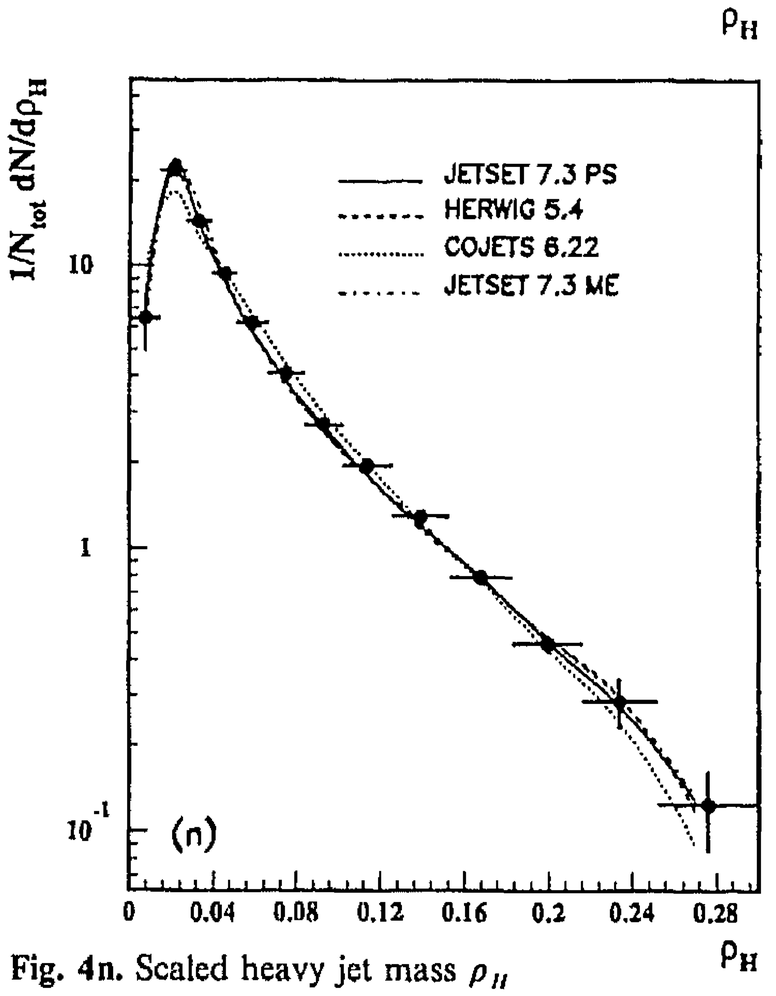

Fig. 4n. Scaled heavy jet mass ρ_H

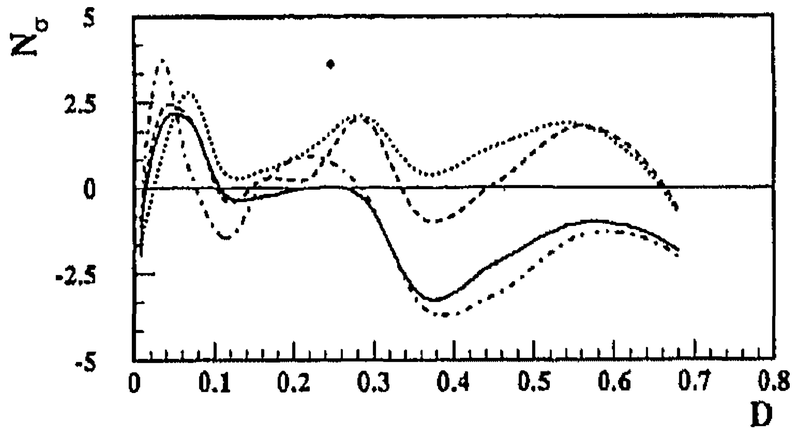

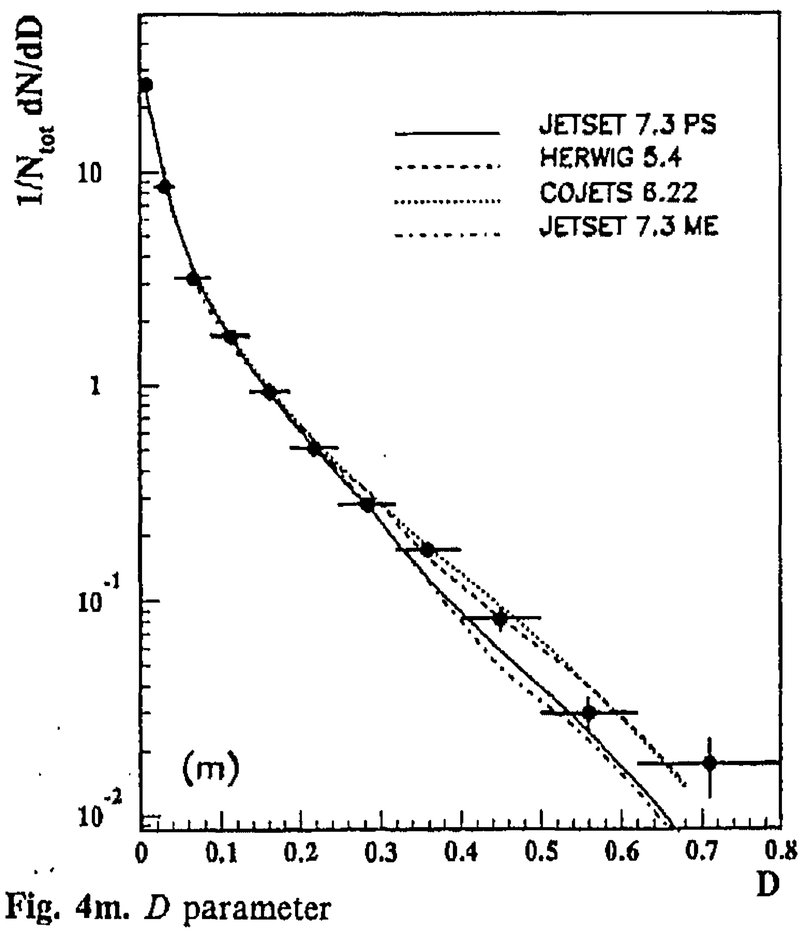

Fig. 4m. D parameter

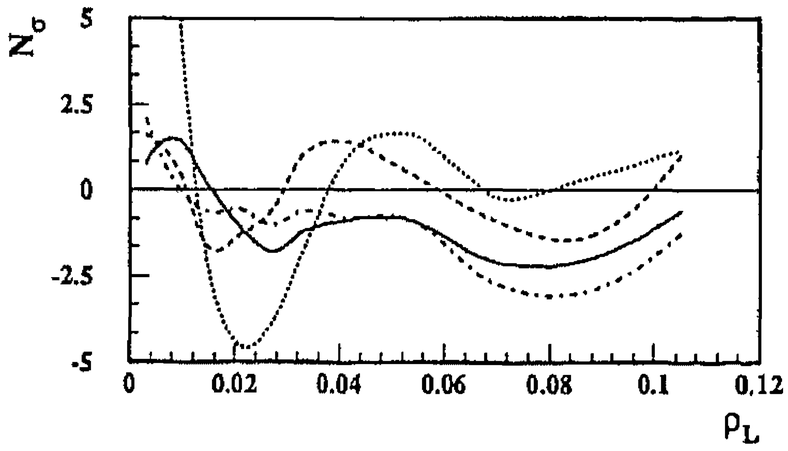

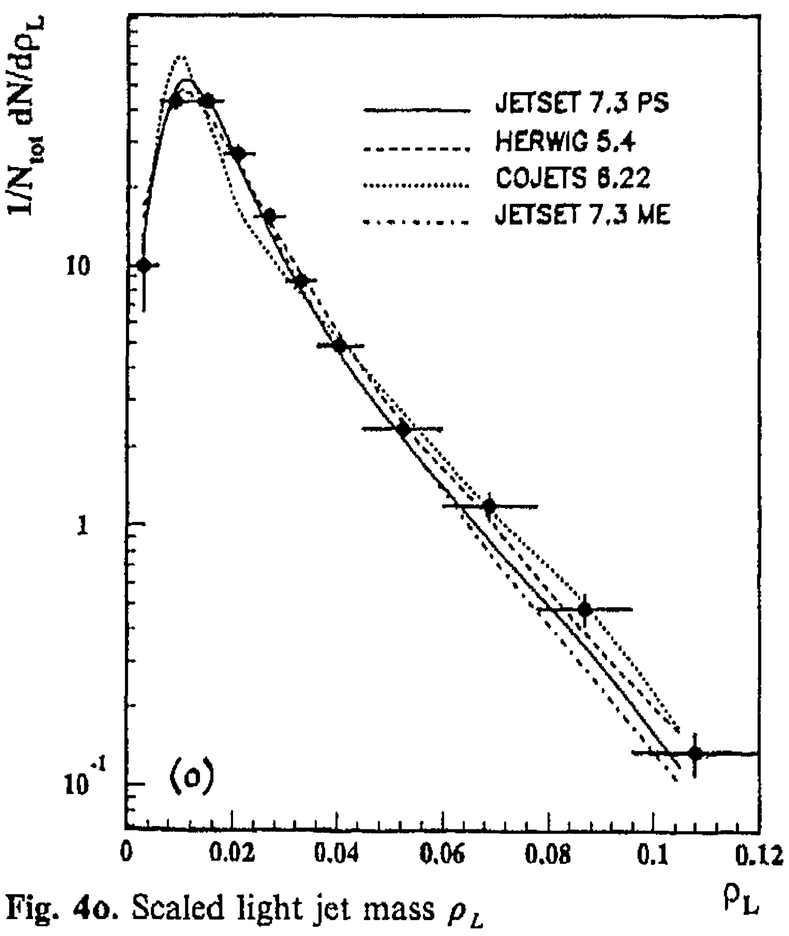

Fig. 4o. Scaled light jet mass ρ_L

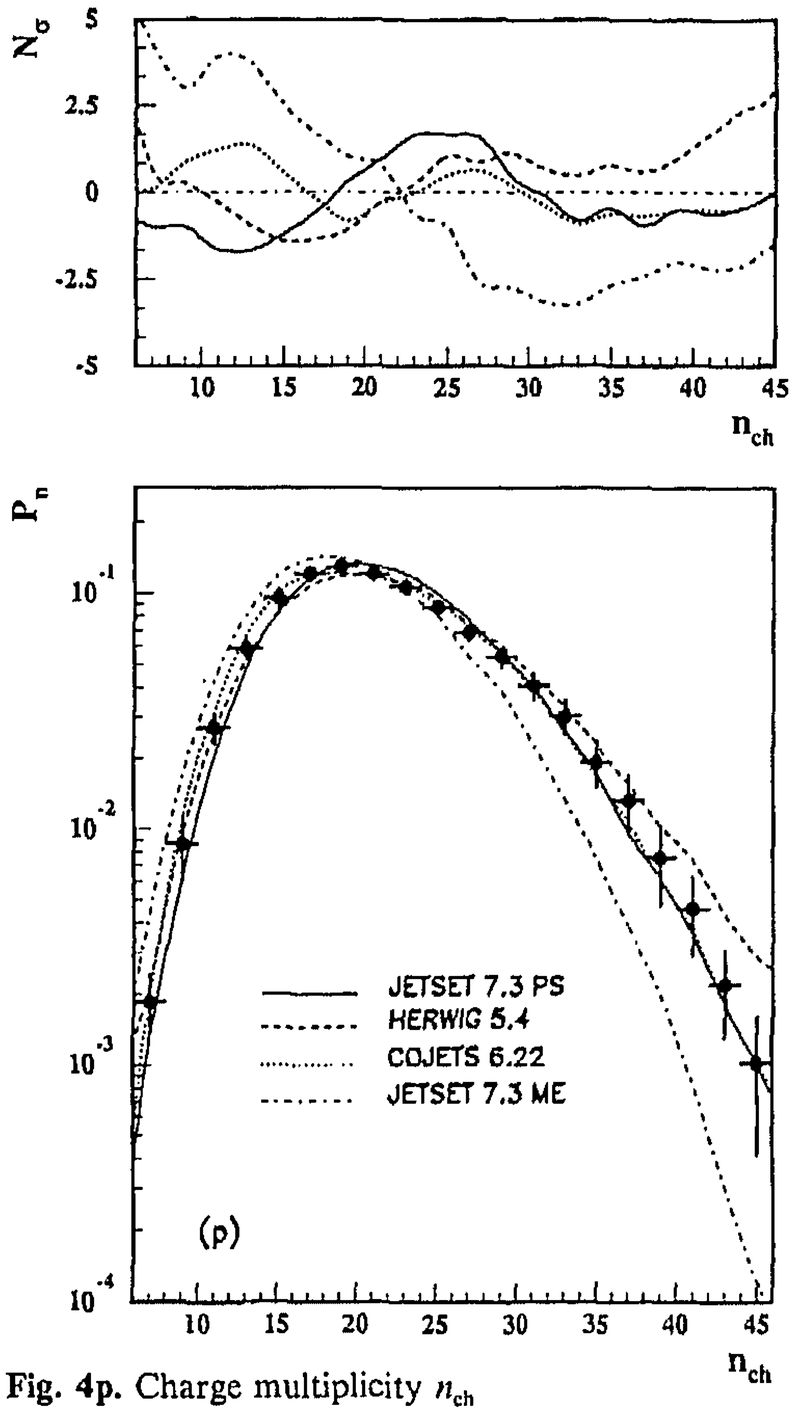

Fig. 4p. Charge multiplicity n_{ch}

The predicted distributions of the event shape variables by NLLJET 2.0 are very close to those of JETSET 7.3 PS and ARIADNE 3.3 in the regions associated with 2- or 3-jet production. In the regions predominantly determined by multi-jet production, the NLLJET 2.0 predictions are lower than those of JETSET 7.3 PS and ARIADNE 3.3, and they do not agree with the data well. In fact, the disagreements between the data and the predictions in these regions contribute most of the total χ^2. NLLJET 2.0 produces 6.5 partons on average and its distributions before hadronization have the same characteristics as those of ARIADNE 3.3. NLLJET 2.0, however, predicts $\langle n_{ch} \rangle$ to be 21.8 after fragmentation.

The JETSET 7.3 ME overestimates the narrow 2-jet production rate while it systematically underestimates the rates for production of four or more jets. It does not reproduce the measured n_{ch} distribution. The predicted $\langle n_{ch} \rangle$ is 18.9. The deficits in the multi-jet production rate are expected since the $O(\alpha_s^2)$ calculations used by the model can produce no more than four partons, with 3.6 partons on average. There is, therefore, no mechanism for production of five or more jets or for soft gluon radiation. The discrepancies in the 2-jet regions can be attributed to the fact that collinear gluon radiation is absent in the model due to the finite recombination parameter y_{min}. Instead, the JETSET 7.3 ME program relies on the fragmentation process to compensate for the low multi-jet rate and for the effects of gluon radiation in the soft as well as in the hard and collinear regions. As a result, the hadronization effects are quite large for most of the variables under study. For example, the predicted M_{ns} distribution is determined completely by hadronization since M_{ns} is always zero with a maximum of four partons before the hadronization.

The JETSET 7.3 PS, ARIADNE 3.3, NLLJET 2.0, and JETSET 7.3 ME programs all use the string fragmentation model. As evident in the minor T_{minor}, aplanarity A, and other distributions, the predictions of these programs follow the same trend. Therefore, it is essential to compare the predictions between Monte Carlo programs using different fragmentation models. The HERWIG 5.4 Monte Carlo program employs the cluster fragmentation model. In the multi-jet regions of the variables M_{ns}, A, D, and ρ_L, the HERWIG predictions are in better agreement with the data than are JETSET 7.3 PS, ARIADNE 3.3 and NLLJET 2.0. These differences in the predictions are likely caused by the differences in the approaches of the parton shower formalisms in the Monte Carlo programs since similar differences already exist at the parton level. Like ARIADNE 3.3 and NLLJET 2.0, the predicted distributions of HERWIG 5.4 in the narrow 2-jet regions are higher than those of JETSET 7.3 PS. The average number of partons and charged tracks predicted by HERWIG 5.4 are 5.8 and 21.6 respectively. At the high tail of the n_{ch} distribution, the HERWIG 5.4 curve is high relative to the measurements.

The COJETS 6.22 program does not describe well the variables which are closely related to the transverse structure of the events, for example oblateness O and scaled light jet mass ρ_L distributions. The model predicts too many transverse-symmetric events. The discrepancy is partially due to the fact that the parameters sensitive to the transverse momentum spectra of the particles are not optimized. The model also fails to describe the data in the 2-jet regions as can be seen, for example, in T_{major} and y_{23}^{JADE} distributions. The model predicts too many narrow 2-jet events. This observation can be explained by the fact that COJETS 6.22 produces only 3.8 partons on average. The small number of partons is expected since the default parton shower termination parameter is high (3 GeV) compared to the other parton shower based models under study. The mean charge multiplicity predicted by COJETS 6.22 is 20.6, in good agreement with the data. We note that most of the parton level distributions of COJETS 6.22 are quite different from those of other parton shower programs.

For a consistency check, we also compared the unfolded data from the charged tracks with the predictions of the models using the same parameters values. The total χ^2 are 208, 292, 368, 378, 225, and 541 for 194 data points*, using JETSET 7.3 PS, ARIADNE 3.3, NLLJET 2.0, JETSET 7.3 ME, HERWIG 5.4, and COJETS 6.22, in good agreement with the comparisons using the unfolded distributions from the calorimetric clusters. This demonstrates, again, that there is no important bias in the detector simulation and that these two measurements are consistent.

* The charge multiplicity distribution is not included in the comparison

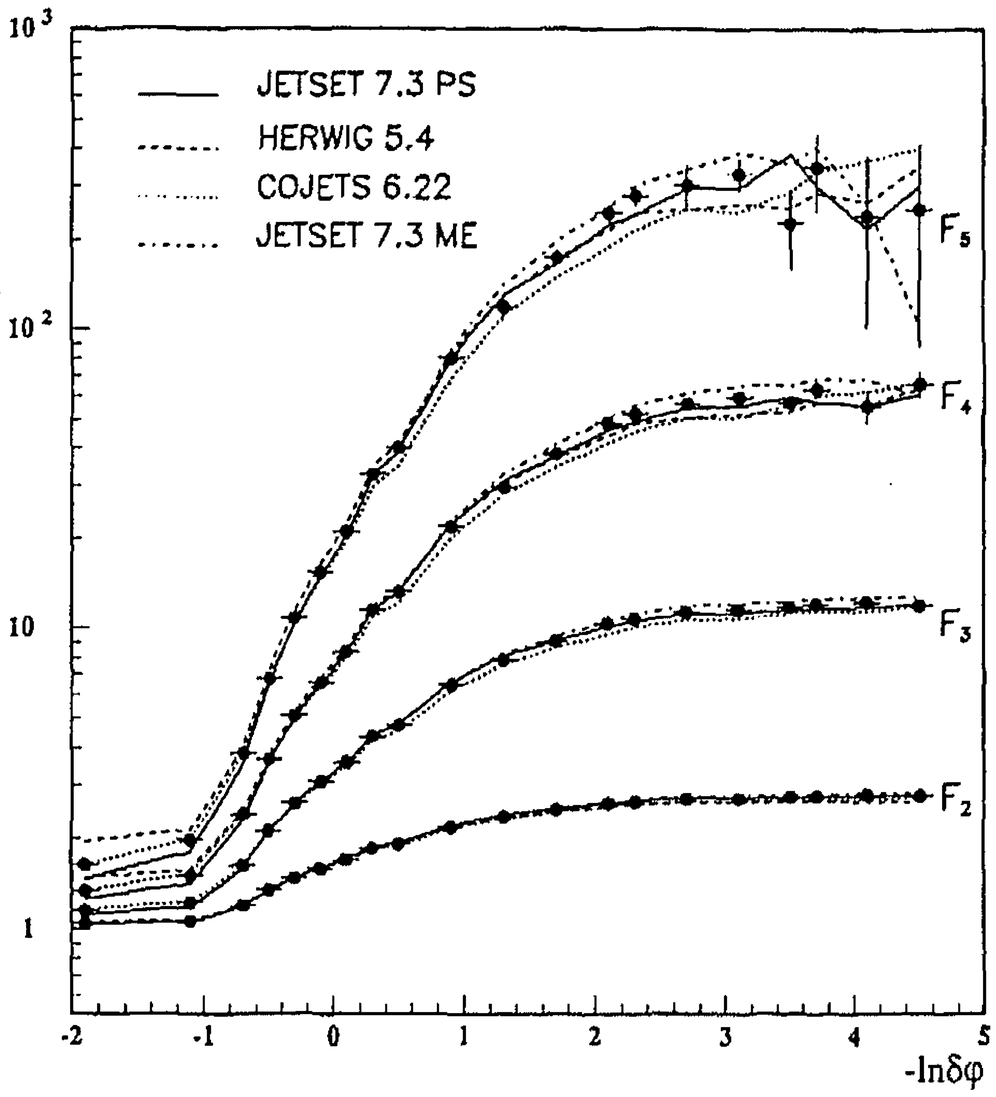

Fig. 5. Comparisons between the corrected 2nd, 3rd, 4th, and 5th factorial moments and the predictions of the JETSET 7.3 PS, HERWIG 5.4, COJETS 6.22, and JETSET 7.3 ME Monte Carlo programs with their optimized parameter values. The dots represent the data, while the lines are the predictions of the Monte Carlo models. The statistical and systematic errors are added in quadrature

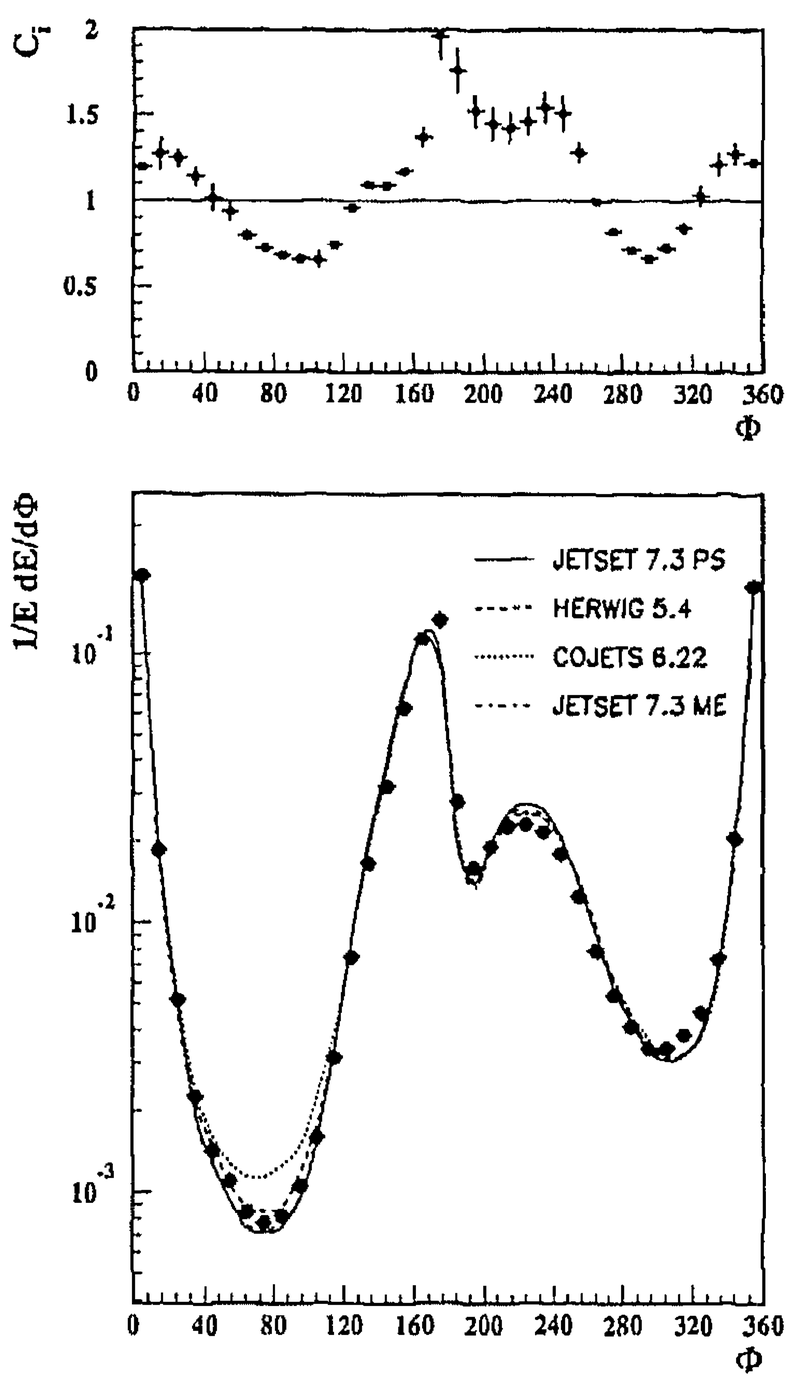

Fig. 6. Comparison between the corrected energy flow distribution and the predictions of the JETSET 7.3 PS, HERWIG 5.4, COJETS 6.22, and JETSET 7.3 ME Monte Carlo programs after optimization. The dots represent the data while the lines are the predictions of the Monte Carlo models. The statistical and systematic errors are added in quadrature. The top insert shows the correction factors derived from the fully detector-simulated JETSET 7.3 PS Monte Carlo events

The measured 2nd, 3rd, 4th, and 5th factorial moments, after correction for detector and radiation effects, are compared with the predictions of the Monte Carlo programs. The comparisons between the data and the distributions of JETSET 7.3 PS, HERWIG 5.4, COJETS 6.22, and JETSET 7.3 ME are shown in Fig. 5. The predictions of ARIADNE 3.3 and NLLJET 2.0 show behavior similar to those of JETSET 7.3 PS and HERWIG 5.4. The factorial moments indeed increase with the increasing resolution in the phase space variable ϕ. The observations are well reproduced by the Monte Carlo models with very different approaches. In other words, the factorial moments are insensitive to the differences in these programs. Similar studies on the Z^0 resonance have been reported in [54].

The corrected energy flow distribution is shown in Fig. 6. Also shown are the predictions of Monte Carlo programs with string (JETSET 7.3 PS and JETSET 7.3 ME), cluster (HERWIG 5.4), and independent (COJETS 6.22) fragmentations. The predicted distributions of ARIADNE 3.3 and NLLJET 2.0 are similar to that of JETSET 7.3 PS. Both parton shower and matrix element based models with string fragmentation describe the depletion in the energy flow distribution well. The data are also well reproduced by the Monte Carlo program with cluster fragmentation. On the other hand, the predictions made by the Monte Carlo program with incoherent parton branching and independent fragmentation in the valley between the first and second most energetic jets are significantly higher than those of other models and are in contradiction with the data.

9 Energy dependences of the mean values

The comparisons between data and the predictions of the QCD models with the optimized parameters at fixed center-of-mass energy provide the first check of the underlying physics of the models. Another important test of the QCD models is to check the predicted energy evolutions of the shape distributions using the same Monte Carlo parameter values.

The mean values of thrust T, spherity S, aplanarity A, and charge multiplicity n_{ch} are shown in Fig. 7a–d, together with other measurements at the Z^0 resonance [50, 55], as well as those at low energy e^+e^- machines [56]. Also shown are the energy dependences of these quantities as predicted by the JETSET 7.3 PS, HERWIG

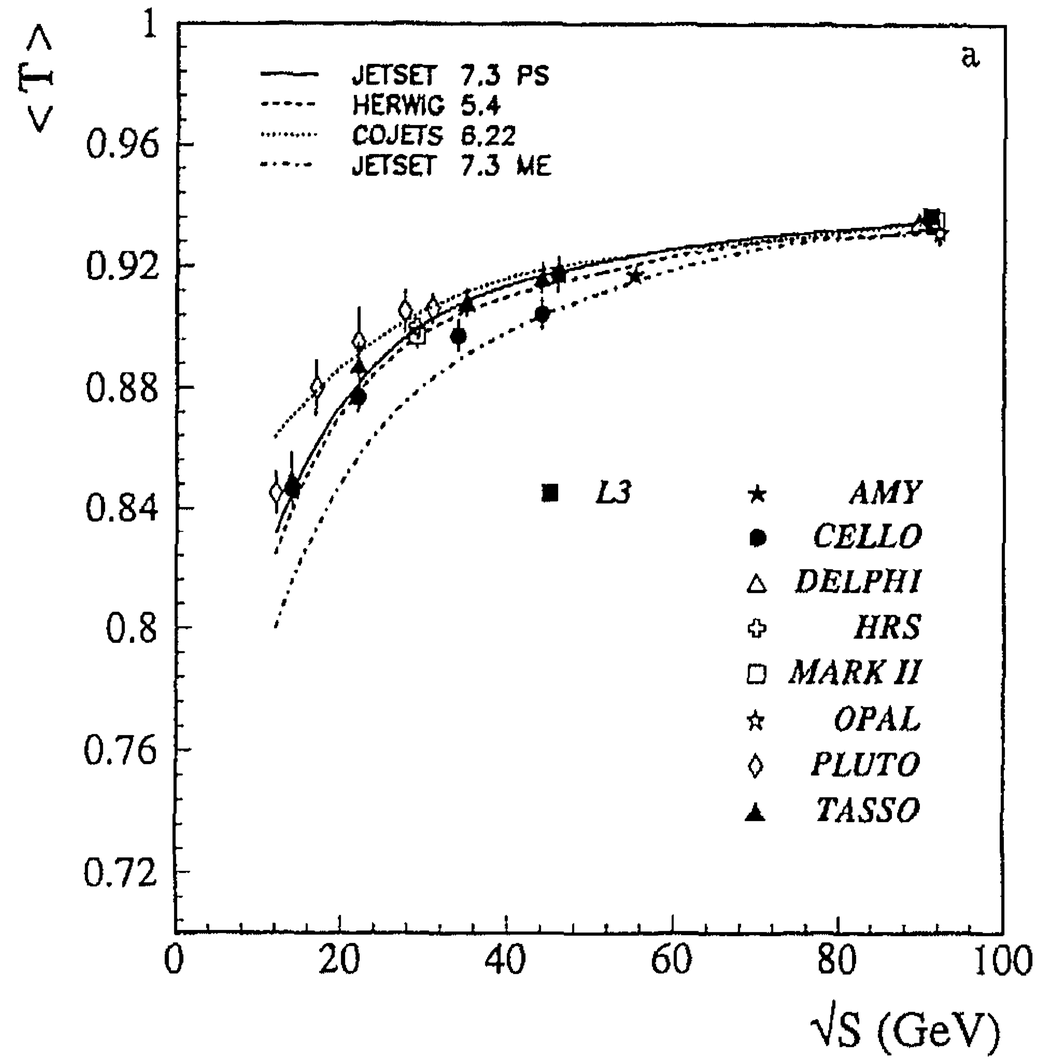

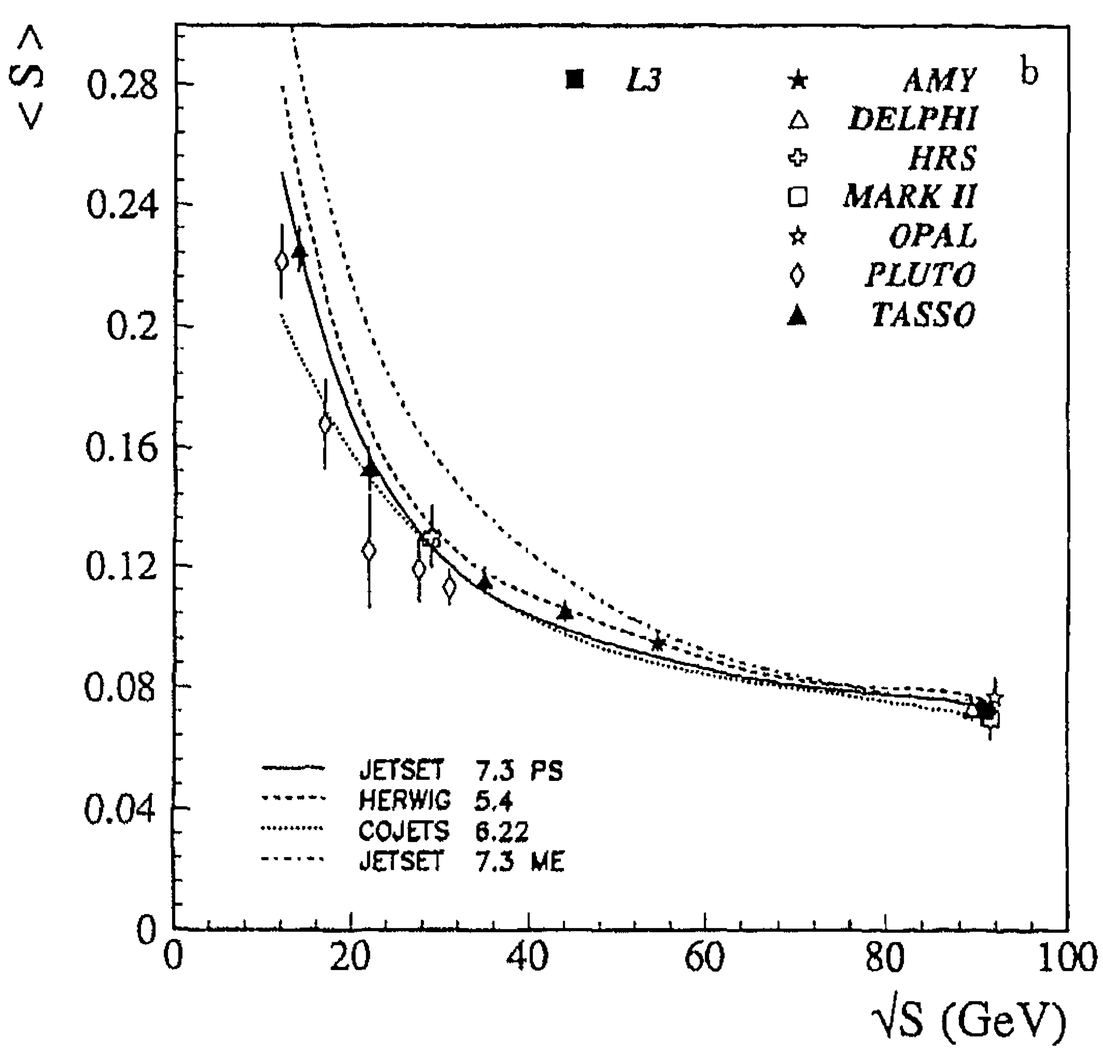

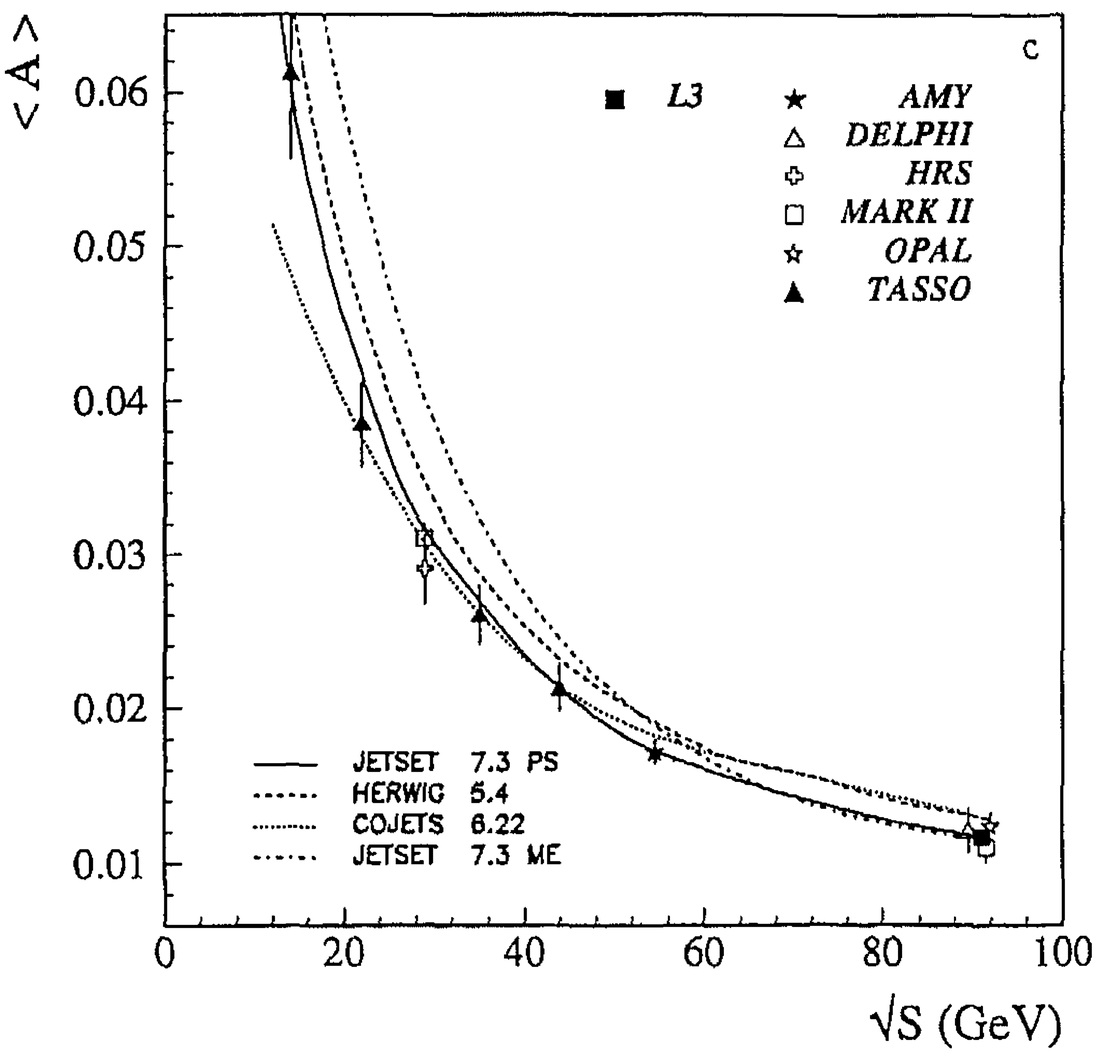

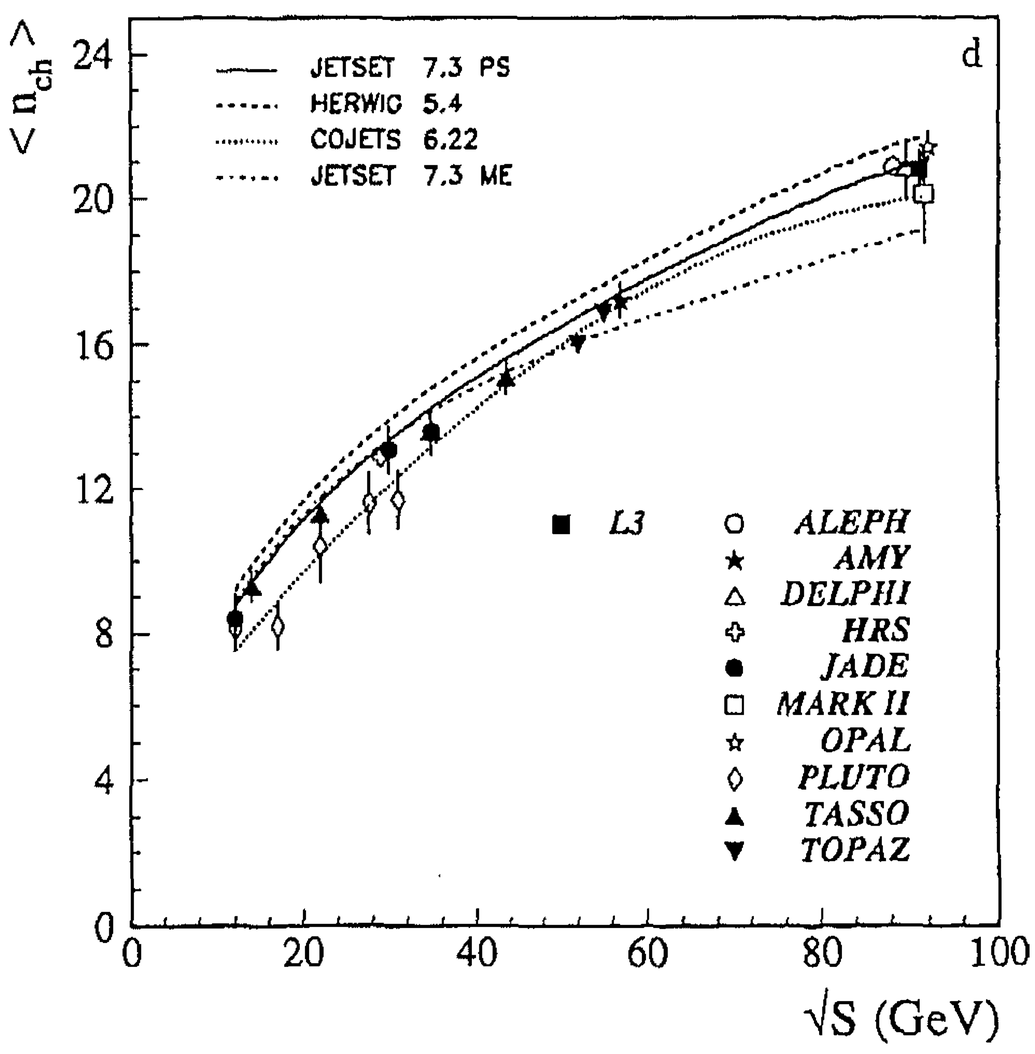

Fig. 7a–d. Comparisons between the mean values of the unfolded data, measured at different center-of-mass energies, and those predicted by the JETSET 7.3 PS, HERWIG 5.4, COJETS 6.22, and JETSET 7.3 ME Monte Carlo models. The Monte Carlo predictions are calculated from the generated events using the same parameter values reported in this paper, for all center-of-mass energies. **a** Thrust $\langle T \rangle$; **b** sphericity $\langle S \rangle$; **c** aplanarity $\langle A \rangle$; **d** charge multiplicity $\langle n_{ch} \rangle$

5.4, COJETS 6.22 and JETSET 7.3 ME Monte Carlo models with constant parameter values over the energy range. The distributions for ARIADNE 3.3 are not shown since they follow closely those of JETSET 7.3 PS.

The energy dependences of these quantities are reproduced by the JETSET 7.3 PS and HERWIG 5.4 models. The predictions of these parton shower based Monte Carlos are generally very similar, especially for the mean values of thrust and sphericity. Nevertheless, the HERWIG 5.4 predictions for the average aplanarity are found to be systematically higher than those of JETSET 7.3 PS and are above most of the data. For the average charge multiplicity, the agreement between data and Monte Carlos is less satisfactory. The model predictions are higher than most of the data points. COJETS 6.22, on the other hand, predicts weaker energy dependences of these mean values. The agreement between the data and its predictions is less satisfactory.

The general trends of the energy evolutions of $\langle T \rangle$, $\langle S \rangle$, $\langle A \rangle$, and $\langle n_{ch} \rangle$ are also predicted by the second order matrix element based program, JETSET 7.3 ME. Although its predictions agree well with some of the data, the JETSET 7.3 ME model fails to describe the energy dependences of $\langle T \rangle$, $\langle S \rangle$, $\langle A \rangle$, and $\langle n_{ch} \rangle$ over a wide energy range. As can be seen in Fig. 7a–d, the predictions often fail to reproduce the data at one end of the energy while reproducing it well at the other end.

10 Summary

We have measured a large number of hadronic event shape variables as well as the factorial moments and the energy flow distribution using a sample of 248 100 hadronic decays of the Z^0. The event shape variables are measured independently using the calorimetric clusters and using the charged tracks. The data are unfolded for detector effects (resolution and acceptance) and for initial and final state photon emission. The results obtained from these two measurements are found to be consistent.

The main parameters of the JETSET 7.3 PS, ARIADNE 3.3, NLLJET 2.0, JETSET 7.3 ME, HERWIG 5.4, and COJETS 6.22 Monte Carlo programs are tuned to describe the measured distributions of the minor of the narrow side M_{ns}, the fourth Fox-Wolfram moment H_4, and the 3-jet resolution parameter of the JADE algorithm y_{23}^{JADE}.

The Monte Carlo predictions with the optimized parameters are compared with the unfolded event shape variables, the factorial moments, and the energy flow distribution. The JETSET 7.3 PS, ARIADNE 3.3, NLLJET 2.0, and HERWIG 5.4 Monte Carlo programs are found to describe the event shape variables in the 2- and 3-jet regions very well. In the regions where the production of four or more jets is important, HERWIG 5.4 gives a slightly better description of the data. The predictions of JETSET 7.3 PS, ARIADNE 3.3, and NLLJET 2.0 in these regions are systematically below the data. The second order matrix element based JETSET 7.3 ME Monte Carlo describes the general structure of the event shape variables well, especially in the regions associated with 3-jet production. Its predictions do not agree well with the data in 2- and multi-jet regions. COJETS 6.22 gives a reasonable description of most of the data in the 2- or 3-jet dominated regions, but it does not provide a satisfactory description for the regions sensitive to transverse momentum spectra.

All the Monte Carlo programs are found to describe the measured factorial moments well. The programs with string or cluster fragmentation give reasonable descriptions of the measured energy flow distribution, while the program with independent fragmentation fails to reproduce the measurement.

We have also studied the energy evolutions of the mean values of thrust T, sphericity S, aplanarity A, and charge multiplicity n_{ch}. The energy dependences of these mean values are well described by the JETSET 7.3 PS, ARIADNE 3.3, NLLJET 2.0, and HERWIG 5.4 Monte Carlos with optimized parameters and they are less well described by COJETS 6.22. The JETSET 7.3 ME Monte Carlo, with fixed parameters, fails to reproduce their energy evolutions.

Acknowledgement. We wish to express our gratitude to the CERN accelerator divisions for the excellent performance of the LEP machine. We acknowledge the effort of all engineers and technicians who have participated in the construction and maintenance of this experiment.

References

1. For a review see: A. Ali, F. Barreiro, in: "High energy electron positron physics", Eds. A. Ali, P. Söding, p. 611. Singapore: World Scientific 1988;
   P. Mättig: Phys. Rep. 177 (1989) 142
2. R. Itoh: "Recent results from TRISTAN", proceedings of joint international lepton-photon symposium and europhysics conference on high energy physics, Geneva, 1991
3. T. Hebbeker: "QCD studies at LEP", proceedings of joint international lepton-photon symposium and europhysics conference on high energy physics, Geneva, 1991
4. L3 Coll., B. Adeva et al.: Nucl. Instrum. Methods A289 (1990) 35
5. For a review see: T. Sjöstrand et al.: Z. Physics at LEP 1, G. Altarelli et al. (eds.), CERN Report CERN-89-08, Vol. 3 (1989) 143
6. K. Konishi, A. Ukawa, G. Veneziano: Nucl. Phys. B157 (1979) 45; R. Odorico: Nucl. Phys. B172 (1980) 157; G.C. Fox, S. Wolfram: Nucl. Phys. B168 (1980) 285; T.D. Gottschalk: Nucl. Phys. B214 (1983) 201; G. Marchesini, B.R. Webber: Nucl. Phys. B238 (1984) 1; B.R. Webber: Nucl. Phys. B238 (1984) 492
7. J. Kalinowski, K. Konishi, T.R. Taylor: Nucl. Phys. B181 (1981) 221; J. Kalinowski et al.: Nucl. Phys. B181 (1981) 253; J.F. Gunion, J. Kalinowski: Phys. Rev. D29 (1984) 1545; J.F. Gunion, J.Kalinowski, L. Szymanowski: Phys. Rev. D32 (1985) 2303
8. X. Artru, G. Mennessier: Nucl. Phys. B70 (1974) 93; B. Andersson, G. Gustafson, T. Sjöstrand: Z. Phys. C – Particles and Fields 6 (1980) 235; B. Andersson et al.: Phys. Rep. 97 (1983) 31
9. R.D. Field, S. Wolfram: Nucl. Phys. B213 (1983) 65
10. A. Krzywicki, B. Petersson: Phys. Rev. D6 (1972) 924; J. Finkelstein, R. Peccei: Phys. Rev. D6 (1972) 2606; F. Niedermayer: Nucl. Phys. B79 (1974) 355; A. Casher, J. Kogut, L. Susskind: Phys. Rev. D10 (1974) 732
11. R.D. Field, R.P. Feynman: Nucl. Phys. B136 (1978) 1
12. JADE Coll., W. Bartel et al.: Phys. Lett. B101 (1981) 129; JADE Coll., W. Bartel et al.: Z. Phys. C – Particles and Fields 21 (1983) 37
13. OPAL Coll., M.Z. Akrawy et al.: Phys. Lett. B261 (1991) 334
14. JETSET 7.3 Monte Carlo program:
    T. Sjöstrand: Comput. Phys. Commun. 39 (1986) 347;
    T. Sjöstrand, M. Bengtsson: Comput. Phys. Commun. 43 (1987) 367
15. ARIADNE 3.3 Monte Carlo program:
    U. Pettersson: ARIADNE: A Monte Carlo for QCD cascades in the color dipole formulation. Lund Preprint, LU TP 88-5 (1988); L. Lönnblad: The colour dipole cascade model and the Ariadne program. Lund Preprint, LU TP 91-11 (1991)
16. NLLJET 2.0 Monte Carlo program:
    K. Kato, T. Munehisa: Phys. Rev. D36 (1987) 61; K. Kato, T. Munehisa: Comput. Phys. Commun. 64 (1991) 67
17. HERWIG 5.4 Monte Carlo program:
    G. Marchesini, B. Webber: Nucl. Phys. B310 (1988) 461; I.G. Knowles: Nucl. Phys. B310 (1988) 571; G. Marchesini et al.: Comput. Phys. Commun. 67 (1992) 465
18. COJETS 6.22 Monte Carlo program:
    R. Odorico: Nucl. Phys. B228 (1983) 381; R. Odorico: Comput.

Phys. Commun. 32 (1984) 139, Erratum: 34 (1985) 43; R. Mazzanti, R. Odorico: Nucl. Phys. B370 (1992) 23; R. Mazzanti, R. Odorico: Bologna preprint DFUB 92/1
19. F.A. Berends, R. Kleiss, S. Jadach: Nucl. Phys. B202 (1982) 63; F.A. Berends, R. Kleiss, S. Jadach: Comput. Phys. Commun: 29 (1983) 185
20. L3 Coll., B. Adeva et al.: Z. Phys. C – Particles and Fields 51 (1991) 179
21. C. Peterson et al.: Phys. Rev. D27 (1983) 105
22. L3 Coll., B. Adeva et al.: Phys. Lett. B261 (1991) 177
23. R.K. Ellis, D.A.Ross, E.A. Terrano: Nucl. Phys. B178 (1981) 421
24. P.M. Stevenson: Phys. Rev. D23 (1981) 2916
25. S.Bethke: Z. Phys. C – Particles and Fields 43 (1989) 331
26. DELPHI Coll., P. Abreu et al.: Phys. Lett. B247 (1990) 167; OPAL Coll., M.Z. Akrawy et al.: Phys. Lett. B235 (1990) 389; OPAL Coll., M.Z. Akrawy et al.: Z. Phys. C – Particles and Fields 49 (1991) 375
27. OPAL Coll., P.D. Acton et al.: Phys. Lett. B276 (1992) 547
28. R.Y. Zhu: MIT Ph.D. thesis (1983)
29. For reviews see:
A. Bassetto, M. Ciafaloni, G. Marchesini: Phys. Rep. 100 (1983) 201; Yu.L. Dokshitzer et al.: Rev. Mod. Phys. 60 (1988) 373; B.R. Webber: Ann. Rev. Nucl. Part. Sci. 36 (1986) 253
30. A. Bassetto, M. Ciafaloni, G. Marchesini: Phys. Lett. B83 (1979) 207; G. Marchesini, L. Trentadue, G. Veneziano: Nucl. Phys. B181 (1981) 335
31. S. Brandt et al.: Phys. Lett. 12 (1964) 57; E. Fahri: Phys. Rev. Lett. 39 (1977) 1587
32. MARK-J Coll., D.P. Barber et al.: Phys. Rev. Lett. 43 (1979) 830
33. MARK-J Coll., D.P. Barber et al.: Phys. Lett. B89 (1979) 139
34. JADE Coll., W. Bartel et al.: Z. Phys. C – Particles and Fields 33 (1986) 23; JADE Coll., S. Bethke et al.: Phys. Lett. B213 (1988) 235
35. Y.L. Dokshitzer: Contribution to the workshop on jets at LEP and HERA, Durham (1990); N. Brown, W.J. Stirling: Z. Phys. C – Particles and Fields 53 (1992) 629; S. Catani et al.: Phys. Lett. B269 (1991) 432; S. Bethke et al.: Nucl. Phys. B370 (1992) 310
36. G.C. Fox, F. Wolfram: Phys. Rev. Lett. 41 (1978) 1581; G.C. Fox, F. Wolfram: Nucl. Phys. B149 (1979) 413; G.C. Fox, F. Wolfram: Phys. Lett. B82 (1979) 134
37. J.D. Bjorken, S.J. Brodsky: Phys. Rev. D1 (1970) 1416
38. G. Parisi: Phys. Lett. B74 (1978) 65; J.F. Donoghue, F.E. Low, S.Y. Pi: Phys. Rev. D20 (1979) 2759
39. T. Chandrahoman, L. Clavelli: Nucl. Phys. B184 (1981) 365; Mark II Coll., A. Peterson et al.: Phys. Rev. D37 (1988) 1; TASSO Coll., W. Braunschweig et al.: Z. Phys. C – Particles and Fields 45 (1989) 11
40. Z. Kunszt, P. Nason: "Z Physics at LEP 1", G. Altarelli et al. (eds.). CERN Report CERN-89-08, Vol. 1 (1989) 373
41. JACEE Coll., T.H. Burnett et al.: Phys. Rev. Lett. 50 (1983) 2062; EHS/NA22 Coll., I.V. Ajinenko et al.: Phys. Lett. B185 (1987) 200; EHS/NA22 Coll., I.V. Ajinenko et al.: Phys. Lett. B222 (1989) 306
42. A. Białas, R. Peschanski: Nucl. Phys. B273 (1986) 703
43. B. Andersson, G. Gustafson, T. Sjöstrand: Phys. Lett. B94 (1980) 211; A.H. Mueller: Phys. Lett. B104 (1981) 161
44. R. Burn et al.: GEANT3 User's Guide, CERN/DD/EE/84.1
45. H. Fesefeldt: RWTH Aachen report PITHA 85/02 (1985)
46. RUN – regularized unfolding program:
V. Blobel: "Unfolding methods in high-energy physics experiments", DESY Report 84-118
47. L3 Coll., B. Adeva et al.: Phys. Lett. B259 (1991) 199
48. L3 Coll., B. Adeva et al.: Phys. Lett. B248 (1990) 464
49. OPAL Coll., M.Z. Akrawy et al.: Z. Phys. C – Particles and Fields 47 (1990) 505
50. ALEPH Coll., D. Decamp et al.: Phys. Lett. B273 (1991) 181; DELPHI Coll., P. Abreu et al.: Z. Phys. C – Particles and Fields 52 (1991) 271; DELPHI Coll., P. Abreu et al.: CERN Preprint CERN-PPE/91-181; OPAL Coll., P.D. Acton et al.: Z. Phys. C – Particles and Fields 53 (1992) 535; OPAL Coll., P.D. Acton et al.: CERN Preprint CERN-PPE/92-18
51. F. James, M. Roos: MINUIT manual, CERN-D506 (1989)
52. L3 Coll., B. Adeva et al.: Phys. Lett. B257 (1991) 469
53. R. Odorico: private communication
54. ALEPH Coll., D. Decamp et al.: Phys. Lett. B273 (1991) 181; DELPHI Coll., P. Aarnio et al.: Phys. Lett. B247 (1990) 137; OPAL Coll., M.Z. Akrawy et al.: Phys. Lett. B262 (1991) 351
55. MARK II Coll., G.S. Abrams et al.: Phys. Rev. Lett. 63 (1989) 1558; MARK II Coll., G.S. Abrams et al.: Phys. Rev. Lett. 64 (1990) 1334
56. AMY Coll., Y.K. Li et al.: Phys. Rev. D41 (1990) 2675; AMY Coll., H.W. Zheng et al.: Phys. Rep. D42 (1990) 737; CELLO Coll., H.J. Behrend et al.: Z. Phys. C – Particles and Fields 44 (1989) 63; HRS Coll., D. Bender et al.: Phys. Rev. D31 (1985) 1; HRS Coll., D. Bender et al.: Phys. Rev. D34 (1986) 3304; JADE Coll., W. Bartel et al.: Z. Phys. C – Particles and Fields 20 (1983) 187; MARK II Coll., A. Peterson et al.: Phys. Rev. D37 (1988) 1; PLUTO Coll., C. Berger et al.: Phys. Lett. B95 (1980) 313; PLUTO Coll., C. Berger et al.: Z. Phys. C – Particles and Fields 12 (1982) 297; TASSO Coll., W. Braunschweig et al.: Z. Phys. C – Particles and Fields 45 (1989) 193; TASSO Coll., W. Braunschweig et al.: Z. Phys. C – Particles and Fields 47 (1990) 187; M. Yamauchi (TOPAZ Coll.): Recent results from TOPAZ at TRISTAN. 24th int. conf. on high energy physics, Munich 1988